ACS Partner Journal
PRECISION CHEMISTRY
pubs.acs.org/PrecisionChem

Review

Recent Advances in Spin-coating Precursor Mediated Chemical Vapor Deposition of Two-Dimensional Transition Metal Dichalcogenides

Dingyi Shen,[‡] Yejun Jin,[‡] Zucheng Zhang, Rong Song, Miaomiao Liu, Wei Li, Xin Li, Ruixia Wu, Bo Li, Jia Li, Bei Zhao,* and Xidong Duan*

Cite This: *Precis. Chem.* 2024, 2, 282−299

Read Online

ACCESS | Metrics & More | Article Recommendations

ABSTRACT: Two-dimensional (2D) transition metal dichalcogenides (TMDs) have garnered widespread interest in the scientific community and industry for their exceptional physical and chemistry properties, and great potential for applications in diverse fields including (opto)electronics, electrocatalysis, and energy storage. Chemical vapor deposition (CVD) is one of the most compelling growth methods for the scalable growth of high-quality 2D TMDs. However, the conventional CVD process for synthesis of 2D TMDs still encounters significant challenges, primarily attributed to the high melting point of precursor powders, and achieving a uniform distribution of precursor atmosphere on the substrate to obtain controllable smaple domains is difficult. The spin-coating precursor mediated chemical vapor deposition (SCVD) strategy provides refinement over traditional methods by eliminating the use of solid precursors and ensuring a more clean and uniform distribution of the growth material on the substrate. Additionally, the SCVD process allows fine-tuning of material thickness and purity by manipulating solution composition, concentration, and the spin coating process. This Review presents a comprehensive summary of recent advances in controllable growth of 2D TMDs with a SCVD strategy. First, a series of various liquid precursors, additives, source supply methods, and substrate engineering strategies for preparing atomically thin TMDs by SCVD are introduced. Then, 2D TMDs heterostructures and novel doped TMDs fabricated through the SCVD method are discussed. Finally, the current challenges and perspectives to synthesize 2D TMDs using SCVD are discussed.

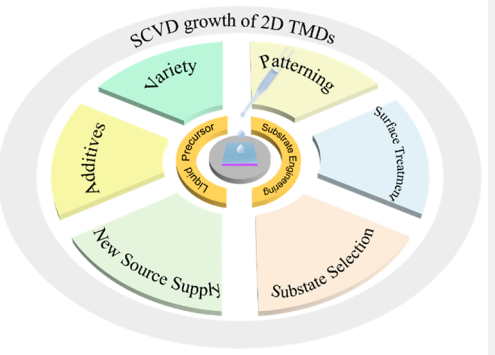

KEYWORDS: *Spin-coating, Chemical vapor deposition, Liquid precursor, Substrate, Two-dimensional materials, Heterostructure, Doping, Film*

1. INTRODUCTION

The discovery of graphene[1] marked a significant milestone in two-dimensional (2D) materials research. Since then, other 2D materials, including transition metal dichalcogenides (TMDs), with the formula MX_2 (M: transition metal atom; X: chalcogen atom), have garnered considerable interest in various fields such as electronics, optoelectronics, magnetics, and catalysis research due to their ultrathin thickness, unique crystal structures, excellent physical and chemical properties.[2−10] It is widely recognized that material preparation is a fundamental prerequisite for meeting the increasing demands of various applications. Therefore, the exploration of diverse synthesis methods for materials is crucial. Conventional mechanical exfoliation methods prove to be inadequate in fulfilling the demands for the precise construction of large-area thin films and heterostructures of 2D TMDs, rendering them unsuitable for practical applications.

Chemical vapor deposition (CVD) method stands out as a preferred method for the synthesis of 2D TMDs and their heterostructures due to relatively good controllability, high quality, and high yield of samples. However, controlling the gas phase distribution and reaction rate of the gas phase during the traditional CVD growth process presents a challenge. The nonuniform distribution of the precursor concentration on the substrate will directly affect the nucleation sites, resulting in undesirable nucleation and poor control of the nucleation density. Research indicates that incorporating additives into the CVD process can lower the melting point of solid

Special Issue: Precision Chemistry for Two-Dimensional Materials

Received: November 29, 2023
Revised: January 18, 2024
Accepted: January 24, 2024
Published: February 13, 2024

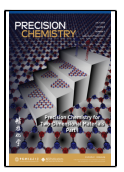

https://doi.org/10.1021/prechem.3c00115
Precis. Chem. 2024, 2, 282−299

precursors and enhance source delivery. For instance, the incorporation of salt additives with metal oxides has been utilized to form intermediate volatile compounds, which can reduce the reaction temperature and promote the reaction.[11,12] However, this method introduces unwanted and unavoidable byproducts or impurities, leading to a notable reduction in the quality of ultrathin TMDs, which affects their stability and results in poor electrical and optical performance.[13,14]

To address this issue, an updated CVD synthesis technique termed spin-coating-mediated precursor chemical vapor deposition (SCVD) is gradually coming into view for the growth of TMDs and has made rapid progress in recent years. In SCVD, one or multiple suitable precursors are dissolved in solvents to form uniform mixed solutions serving as metal-containing sources. Subsequently, the precursor solutions are spin-coated onto the pretreated substrates, reacting with chalcogen to produce 2D TMDs. And the thickness of the synthesized 2D TMDs can be regulated by adjusting the concentration of solution and spin coating speed. As the synthesis process involves heating, the solutes gradually transform into a molten liquid state, facilitating more complete reactions with chalcogen feedings. Unlike the conventional CVD growth method where the positioning of substrates with precursors is crucial, SCVD method enables direct reaction and nucleation on the substrate, which eliminates the issues related to position-dependent substrates with precursors and reduces the formation of undesirable byproducts and additional contaminants during growth. It enables precise control of the precursor atmosphere, ensuring a clean and uniform distribution of the resulting sample on the substrate, thus achieving controllability and repeatability of material preparation. It is worth noting that SCVD technology is particularly advantageous for synthesizing large-area single-layer or multilayer TMD thin films. For example, the liquid precursor $(NH_4)_6H_2W_{12}O_{40}\cdot x(H_2O)$ (AMT) was reported to be deposited on Au to synthesize WS_2 monolayers with domain sizes up to ∼420 μm.[15] The wafer-scale MoS_2 layers were obtained through thermolysis of a spin-coated $(NH_4)_2MoS_4$ solution film.[16] Furthermore, by regulating the tunable doping concentrations of various dopants in mixed solutions, the properties and functionalities of 2D TMDs can be engineered. Overall, TMDs grown by SCVD have the advantages of precise controllability of composition, thickness, and other key parameters.

Herein, we present the recent advancements in controllable SCVD growth of 2D TMDs. The first part focuses on the exploration of liquid precursors of SCVD, and introduces the different kinds of liquid precursors, additives, and new source supply methods, such as bubble method, dissolution−precipitation method, and monomer feeding method. The second part discusses the substrate engineering strategies including substrate choice, surface treatment, and patterning. It is worth noting that substrate engineering plays a crucial role in controlling the nucleation and growth of TMD films. The third part mainly introduces 2D TMDs heterostructures and the novel doped TMDs in the SCVD. Finally, we provide insights into the challenges and potential opportunities for fabricating and commercializing 2D TMDs using SCVD in the future.

2. SCVD GROWTH OF 2D TMDs

Nowadays, the SCVD technique has demonstrated its superiority in synthesizing 2D TMDs with excellent reproducibility and homogeneity under mild conditions. In this section, our primary focus is on the liquid precursor categories, additives, and new source supply method in SCVD. And the implementation of effective substrate pretreatment strategies can significantly increase the size of the synthesized material, potentially extending it to the centimeter level even to the wafer-level films.

2.1. Liquid Precursors for SCVD

2.1.1. Importance of Liquid Precursors in Determining TMDs Quality. Utilizing liquid precursors in the SCVD method effectively overcomes the challenge of unstable nucleation that arises from the difficulty in controlling the evaporation of solid precursors in the CVD method. The selection of liquid-phase precursor is a critical factor in the success of SCVD. In addition, a lot of progress has been made in the growth of various 2D TMDs in monolayer and few-layer forms using SCVD.

It is worth summarizing that the precursors generally should (i) have a melting point lower or close to the growth temperature, (ii) be enabled to form stable melts in the reaction, and (iii) be soluble in the target solvent and become stable compounds in solutions. The first two conditions promote the growth of the target material, while the last condition facilitates the formation of a homogeneous solution mixture. In the literature, precursors such as $(NH_4)_2MoS_4$,[17] Na_2MoO_4,[18] Na_2WO_4,[19] $NaReO_4$,[20] and $C_4H_4NNbO_9$[21] have been used for the SCVD growth of 2D TMDs. The possible chemical reactions in SCVD growth of 2D TMDs are illustrated in Table 1.

Table 1. Possible Chemical Reactions in SCVD Growth of 2D TMDs

	Reactions	References
MoS_2	$(NH_4)_2MoO_4 + 4S + 2KOH + H_2O \rightarrow MoO_3 + 3H_2S + K_2SO_4 + 2NH_3$	22
	$2MoO_3 + 7S \rightarrow 2MoS_2 + 3SO_2$	
	$(NH_4)_6Mo_7O_{24}\cdot 4H_2O \rightarrow 6NH_3 + 7H_2O + 7MoO_3$	23
	$2MoO_3 + 7S \rightarrow 2MoS_2 + 3SO_2$	
$MoSe_2$	$2(NH_4)_2MoO_4 \rightarrow 2MoO_3 + 4NH_3 + 2H_2O$	24
	$2MoO_3 + 2KI \rightarrow MoO_2I_2 + K_2MoO_4$	
	$MoO_2I_2 + 4H_2 + 3Se \rightarrow MoSe_2 + 2HI + 2H_2O + H_2Se$	
	$Na_2MoO_4 + 2Na_2SeO_3 + 3Se + 10H_2 \rightarrow MoSe_2 + 3Na_2Se + 10H_2O$	20
WS_2	$(NH_4)_{10}W_{12}O_{41} \rightarrow 10NH_3 + 5H_2O + 12WO_3$	25
	$2WO_3 + 7S \rightarrow 2WS_2 + 3SO_2$	
$MoTe_2$	$Na_2MoO_4 + 3Te + 3H_2O \rightarrow TeO_2 + 2H_2Te + MoO_3 + 2NaOH$	26
	$MoO_3 + 2TeO_2 + 7H_2 \rightarrow MoTe_2 + 7H_2O$	
WTe_2	$Na_2WO_4 + 2Na_2TeO_3 + 3Te + 10H_2 \rightarrow WTe_2 + 3Na_2Te + 10H_2O$	20

In 2012, $(NH_4)_2MoS_4$ solution was dip-coated onto an insulating substrate and subsequently decomposed through high-temperature annealing, resulting in the production large-area MoS_2 thin layers (Figure 1a).[17] However, the dip-coating method frequently results in nonuniform distribution of precursor on the substrate, leading to the formation of multidomains with different layer numbers. To tackle this challenge, Liu et al. utilized a Na_2WO_4 solution as a precursor for spin coating and successfully synthesized monolayer WS_2 crystals after annealing the precursor.[18] Figure 1b displays the OM images of a WS_2 crystal with and without annealing. The precursor annealing process resulted in the redistribution of

https://doi.org/10.1021/prechem.3c00115
Precis. Chem. 2024, 2, 282−299

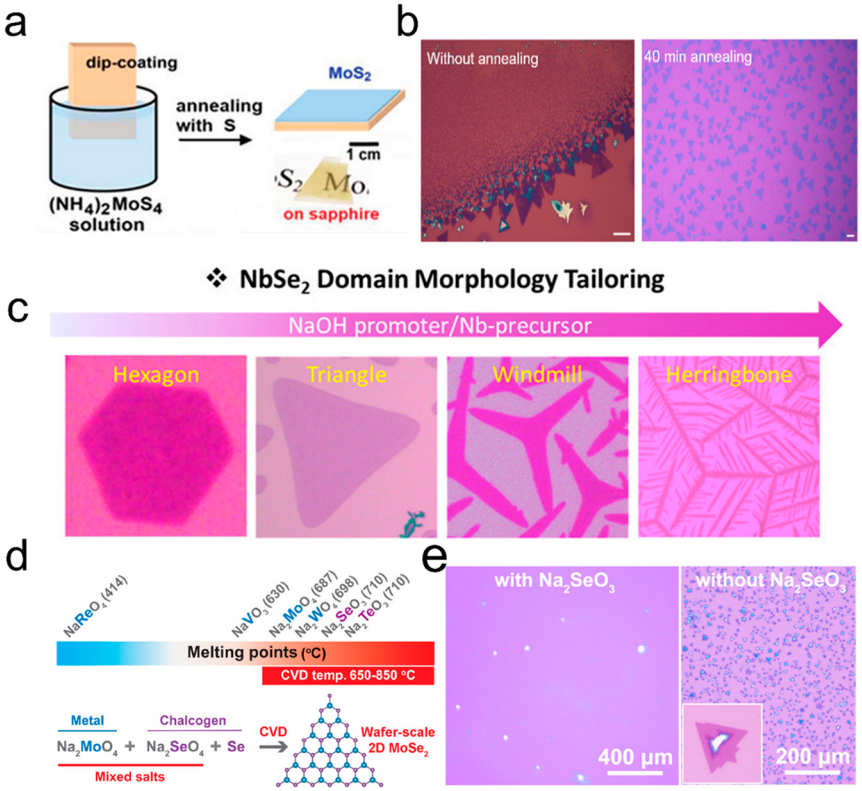

Figure 1. Synthesis of TMDs with SCVD. (a) Schematic illustration of decomposing the dip-coating $(NH_4)_2MoS_4$ to produce multilayer MoS_2. Reproduced from ref 17. Copyright 2012 American Chemical Society. (b) OM image of WS_2 crystal before and after annealing using Na_2WO_4 solution as a precursor; scale bar: 20 μm. Reproduced from ref 18. Copyright 2020 American Chemical Society. (c) Change in the morphology of $NbSe_2$ at various NaOH/$C_4H_4NNbO_9{\cdot}xH_2O$ ratios. Reproduced from ref 21. Copyright 2020 American Chemical Society. (d) Melting points of several precursors and synthetic strategy of $MoSe_2$ with mixed-salt precursors. (e) OM image of $MoSe_2$ monolayer grown with or without adding Na_2SeO_3. The inset shows a typical $MoSe_2$ nanoflake in an area of 10 × 10 μm^2. Reproduced from ref 20. Copyright 2021 American Chemical Society.

the molten liquid precursor, effectively preventing aggregation and promoting monolayer growth. Park et al. utilized mixed solutions of $C_4H_4NNbO_9{\cdot}xH_2O$ with different concentrations to construct the different morphologies of metallic $NbSe_2$ from hexagonal, triangular, windmill-like, to herringbone-like (Figure 1c).[21] The concentration of the Nb precursor gradually increases and surpasses that of the Se precursor. As a result, Se-terminated facets grow faster than Nb-terminated facets under Nb-rich conditions. Monolayer WTe_2 and $MoTe_2$ have also been successfully synthesized using $(NH_4)_6H_2W_{12}O_{40}{\cdot}xH_2O$ and $(NH_4)_6Mo_7O_{24}{\cdot}4H_2O$ as precursors, respectively.[27,28] Various precursors with the formula A_xMO_y (where A is an alkali metal or ammonium and M is a transition metal) have been employed in the growth of TMDs, such as Na_2MoO_4,[19] Na_2WO_4[19] and $(NH_4)_2MoO_4$.[29]

On the other hand, the synthesis of high-quality 2D TMDs is also inseparable from the precise feeding of chalcogen. Similarly, liquid precursors can also be used as a source of chalcogen supply, such as Na_2SeO_3 and Na_2TeO_3. Taniguchi et al. proposed various groups of mixed precursors to synthesis transition metal selenides and tellurides. Figure 1d shows the melting points of several precursors. The 2D $MoSe_2$, $ReSe_2$, and WTe_2 were successfully produced with Na_2MoO_4–Na_2SeO_3, $NaReO_4$–Na_2SeO_3, and Na_2WO_4–Na_2TeO_3 as precursors, respectively.[20] The OM images of the $MoSe_2$ monolayer grown with or without the addition of Na_2SeO_3 are shown in Figure 1e. Despite the SCVD technique being a universal option for growing large groups of 2D TMDs, the limited suitable precursors degrade the versatility of this strategy. Notably, along with 2D TMDs, a group of transition metal carbides (TMNxs) including MoNx, WNx, CrNx, VNx, and transition metal carbides (TMCs) like MoC_2 have been fabricated via SCVD technique,[30,31] which suggests the potential diversification of the 2D material family. The more detailed information regarding synthesized 2D TMDs by SCVD is illustrated in Table 2.

2.1.2. Overview of Additives Used in SCVD Growth.

Many research results indicate that the addition of additives can significantly improve the interaction between the precursor vapor and substrate during the growth of materials.[11,45−47] Here, the additives used during SCVD growth are divided into inorganic and organic compounds for further discussion and analysis.

In recent years, researchers have discovered that inorganic additives play multifaceted roles in SCVD growth, including growth promotion, acting as reducing agents, and acting as solvents. Notably, additives such as KI and NaOH have been widely studied.

For example, Kong et al. reported that through introducing KI into the $(NH_4)_2MoO_4$ solution, the domain size of synthesized MoS_2 monolayers could reach up to approximately 0.62 mm from vertex to vertex (Figure 2a),[37] which demonstrates the effectiveness of KI as an additive in promoting the growth of large-area monolayer MoS_2. Kim et

https://doi.org/10.1021/prechem.3c00115
Precis. Chem. 2024, 2, 282−299

Table 2. Summary of SCVD Synthesis of 2D TMDs

TMDs	Source materials	Phase	Morphology	Thickness	Temperature (°C)	Substrate	Carrier gas (sccm)	Growth time [min]
MoS_2	$(NH_4)_2MoS_4 + S$[32]	2H	Nanosheet	1.5−2 nm	700	SiO_2/Si	300Ar	14
	$Na_2MoO_4 + NaOH + S$[33]	2H	Nanosheet	2.07 nm	800	Sapphire		2
	$(NH4)_2MoO_4 + KOH + S$[22]	2H	Film	0.7 nm	750	Sapphire/SiO_2/Si	30Ar	10
	$MoO_3 + NH_4OH + S$[34]	2H	Nanosheet	Monolayer	760−880	Glass	150Ar	5
	$(NH_4)_6Mo_7O_{24}{\cdot}4H_2O + S$[35]	2H	Film	0.6−2.5 nm	800	SiO_2/Si	100Ar	10
	$Na_2MoO_4{\cdot}2H_2O + C_{12}H_{25}SH$[36]	2H	Nanosheet	Monolayer	850	SiO_2/Si	10Ar	60
	$(NH_4)_2MoO_4 + KI + S$[37]	2H	Film	1 nm	720	SiO_2/Si	30Ar	3−5
	$(NH_4)_2MoS_4$[17]	2H	Film	2 nm	1000	Sapphire, SiO_2/Si	80%Ar/20% H_2	30
	$(NH_4)_2MoO_4 + S$[29]	2H	Nanosheet	0.78 nm	750	Sapphire	Ar	20
	$(NH_4)_2MoS_4$[38]	2H	Film	2−30 nm	700	SiO_2/Si	96%Ar/4% H_2	60
	$Na_2MoO_4{\cdot}2H_2O + (C_2H_5)_2S$[39]	2H	Film	0.7 nm	850	Sapphire, SiO_2/Si	350Ar/10 H_2	20
	$Na_2MoO_4 + Mo(CO)_6 + CH_3S_SCH_3$[40]	2H	Film	0.9 nm	850	SiO_2/Si	350Ar/15H_2	20
	$MoO_3 + NH_4OH + S$[41]	2H	Film	0.8 nm	800	SiO_2/Si	150Ar	5
	$Na_2MoO_4 + S$[19]	2H	Nanosheet	Monolayer	730−750	soda lime glass slide	80Ar	10−20
	$Na_2MoO_4 + ZnS$[42]	2H	Nanosheet	Monolayer	780	Sapphire/SiO_2/Si	100Ar	10−60
	$(NH4)_2MoO_4 + KI + S$[24]	2H	Film	Monolayer	800	Sapphire	Ar	10
$MoSe_2$	$(NH_4)_2MoO_4 + KI + Se$[24]	2H	Film	Monolayer	800	sapphire	Ar/H_2	10
	$Na_2MoO_4 + Se$[19]	2H	Nanosheet	Monolayer	750−800	soda lime glass slide	80Ar/8 H_2	10−20
	$Na_2MoO_4 + ZnSe$[42]	2H	Nanosheet	Monolayer	800	Sapphire/SiO_2/Si	100Ar	10−60
	$Na_2MoO_4 + Na_2SeO_3$[20]	2H	Nanosheet	Monolayer	775−850	SiO_2/Si	190Ar/10H_2	5−10
WS_2	$(NH_4)_{10}H_2(W_2O_7)_6 + S$[32]	2H	Nanosheet	1.5−2 nm	700	SiO_2/Si	300Ar	14
	$Na_2WO_4{\cdot}H_2O + N_2H_4 + (CH_3)_2S_2$[43]	2H	Film	0.65 nm	850	SiO_2/Si	350Ar	30
	$Na_2WO_4 + S$[19]	2H	Nanosheet	Monolayer	730−780	soda lime glass slide	80Ar/4H_2	10−20
	$Na_2WO_4 + ZnS$[42]	2H	Nanosheet	Monolayer	930	Sapphire/SiO_2/Si	100Ar	10−60
	$(NH_4)_2WO_4 + KI + S$[24]	2H	Film	Monolayer	850	sapphire	Ar/H_2	10
WSe_2	$Na_2WO_4 + ZnSe$[42]	2H	Nanosheet	Monolayer	820	Sapphire/SiO_2/Si	100Ar	10−60
	$(NH_4)_2WO_4 + KI + Se$[24]	2H	Film	Monolayer	850	sapphire	Ar/H_2	10
$MoTe_2$	$Na_2MoO_4 + Te$[19]	1T′	Nanosheet		730−750	soda lime glass slide	120Ar/20H_2;	10−20
	$(NH_4)_6Mo_7O_{24}{\cdot}4H_2O + C_{24}H_{39}NaO_5 + Te$[27]	1T′	Nanosheet	0.8 nm	700/500	SiO_2/Si	400N_2/25H_2;	5
	$Na_2MoO_4 + ZnTe$[42]	2H	Nanosheet	Monolayer	750−800	Sapphire/SiO_2/Si	100Ar	10−60
	$Na_2MoO_4 + ZnTe$[42]	1T′	Nanosheet	Monolayer	800	Sapphire/SiO_2/Si	100Ar	10−60
	$(NH_4)_6Mo_7O_{24} + NaOH + Te$[44]	1T′	Nanosheet	0.82 ± 0.04 nm	730	SiO_2/Si	100Ar/3H_2	15
WTe_2	$Na_2WO_4 + ZnTe$[42]	1T′	Nanosheet	Monolayer	780	Sapphire/SiO_2/Si	100Ar	10−60
	$(NH_4)_6H_2W_{12}O_{40} + Te$[28]	1T′	Nanosheet	0.8 nm	650	SiO_2/Si	N_2/H_2	6
	$Na_2WO_4 + Na_2TeO_3$[20]	1T′	Nanosheet	2.1 nm	775−825	sapphire	95Ar/5H_2	5
$NbSe_2$	$C_4H_4NNbO_9{\cdot}xH_2O + NaOH + Se$[21]	2H	Nanosheet	0.7 nm	800	SiO_2/Si	600N_2/15H_2	20
$ReSe_2$	$NaReO_4 + Na_2SeO_3$[20]	1T′	Nanosheet		750	sapphire	190Ar/10H_2	5−10

al. reported the synthesis of large-area monolayer $MoSe_2$ with good uniformity on 3 cm × 3 cm sapphire substrate via KI promoter assisted as shown in Figure 2b,c.[24] Further research indicates that KI not only facilitates the formation of reactive transition metal oxyhalide, reducing the energy barrier of chalcogenization, but also promotes the growth along the in-plane direction. The addition of KI is also suitable for other TMDs families, including MoS_2, WS_2, and WSe_2. Similarly, centimeter scale $Nb_{1-x}W_xSe_2$ monolayers have been reported with the assistance of promoter KI, allowing for tunable composition to achieve continuously adjustable bandgaps.[48] In another study, Zhao et al. added NaCl salt into $(NH_4)_6Mo_7O_{24}$ (AHM)) solution to achieve rapid growth of large-area monolayer $MoSe_2$ films.[49] Nguyen et al. found that the presence of $NaNO_3$ suppressed nucleation and subsequently increased crystal size significantly. Figure 2d,e shows OM images of MoS_2 nanoflakes with and without $NaNO_3$ catalyst.[50] As illustrated in Figure 2f, $NaNO_3$ reacts with

https://doi.org/10.1021/prechem.3c00115
Precis. Chem. 2024, 2, 282−299

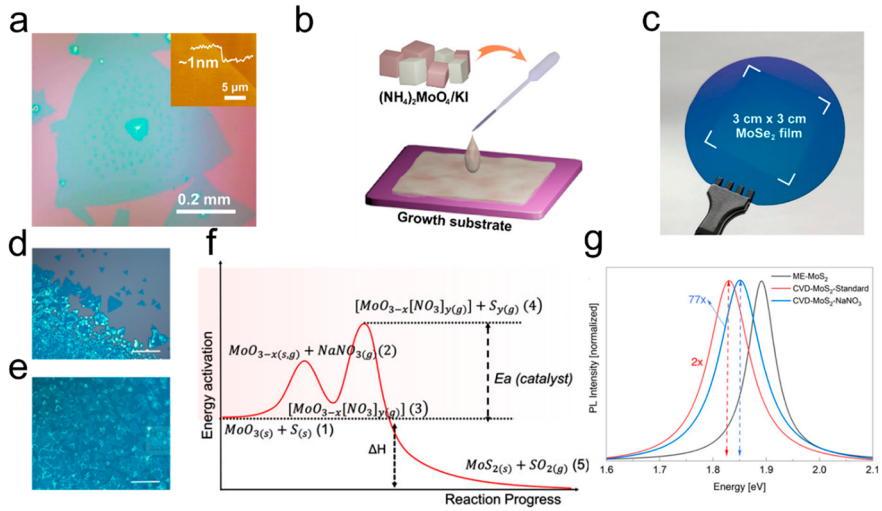

Figure 2. Synthesis of MoS_2 using inorganic additives. (a) OM image of MoS_2 crystal with introducing KI into the $(NH_4)_2MoO_4$ solution precursor, inset is the atomic force microscopy with height of 1 nm. Reproduced from ref 37. Copyright 2021 American Association for the Advancement of Science (AAAS). (b,c) Schematic illustration of mixing $(NH_4)_2MoO_4$/KI liquid precursors (b) to synthesize centimeter-scale monolayer $MoSe_2$ film (c). Reproduced from ref 24. Copyright 2021 American Chemical Society. (d,e) OM image of synthesized MoS_2 monolayers without and with the addition of $NaNO_3$ catalyst. Scale bars: 20 μm. (f) The reaction mechanism of synthesis of MoS_2 monolayers with the addition of $NaNO_3$. (g) Photoluminescence spectra of MoS_2 obtained by mechanical exfoliation and grown by SCVD. Reproduced from ref 50. Copyright 2022 American Chemical Society.

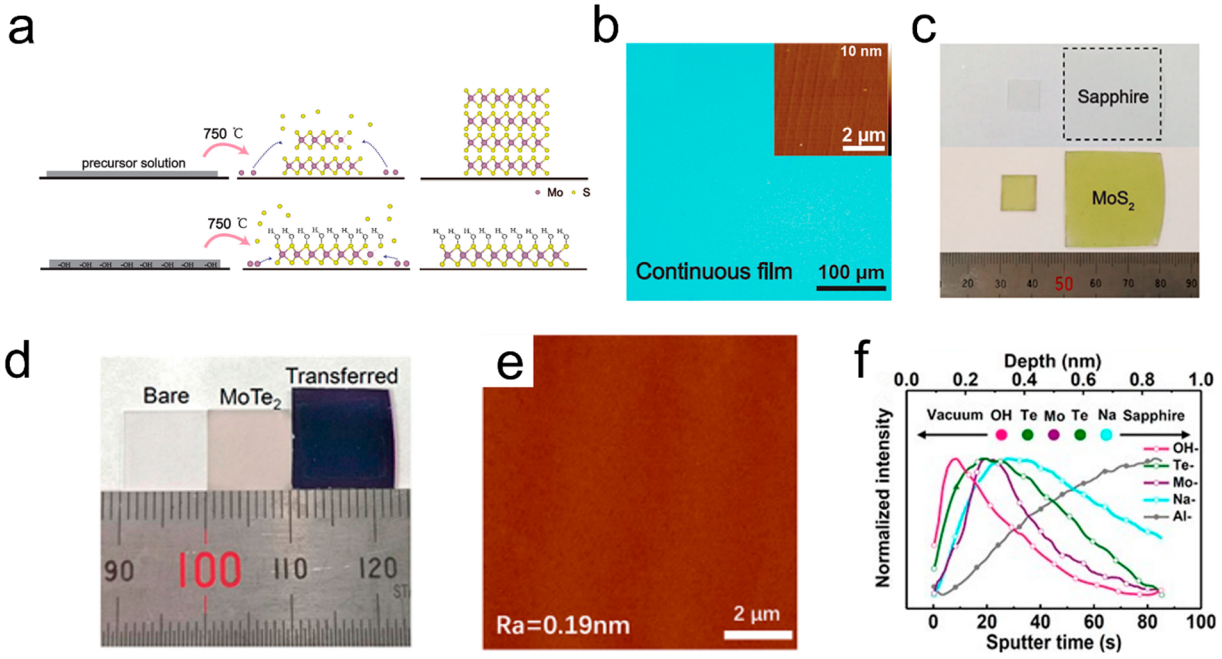

Figure 3. Synthesis of TMDs films using inorganic additives. (a) Schematic mechanism of MoS_2 growth process with −OH or not. (b) OM image of a continuous MoS_2 film grown on sapphire. The inset is an AFM image showing the atomically flat surface. (c) Photographs of 1 × 1 and 3 × 3 cm^2 MoS_2 monolayer films on sapphire. Reproduced from ref 22. Copyright 2019 American Chemical Society. (d) Photograph of 1 cm × 1 cm bare sapphire, as-grown $MoTe_2$ monolayer on sapphire, and transferred $MoTe_2$ monolayer on SiO_2/Si substrate. (e) Typical AFM image of monolayer $MoTe_2$ with small roughness (Ra = 0.19 nm). (f) ToF-SIMS depth profile of the $MoTe_2$−OH sample. Reproduced from ref 26. Copyright 2021 American Chemical Society.

MoO_{3-x} to form a metal oxynitrate $[MoO_{3-x}[NO_3]_y]$, which has a melting point lower than that of the metal oxide, reducing the overall activation energy. The formation of the metal oxynitrate affected the reaction kinetics and expedited the reaction equilibrium, resulting in an increase in the density and size of the MoS_2 monolayers. However, the corresponding PL intensity is significantly reduced due to the presence of excess residues (Figure 2g).

Besides, NaOH(KOH) is also commonly used as an additive because it could improve the uniform distribution of precursors on the substrate, which is important especially in growing centimeter-scale uniform monolayer TMDs films.[33,51]

https://doi.org/10.1021/prechem.3c00115
Precis. Chem. 2024, 2, 282−299

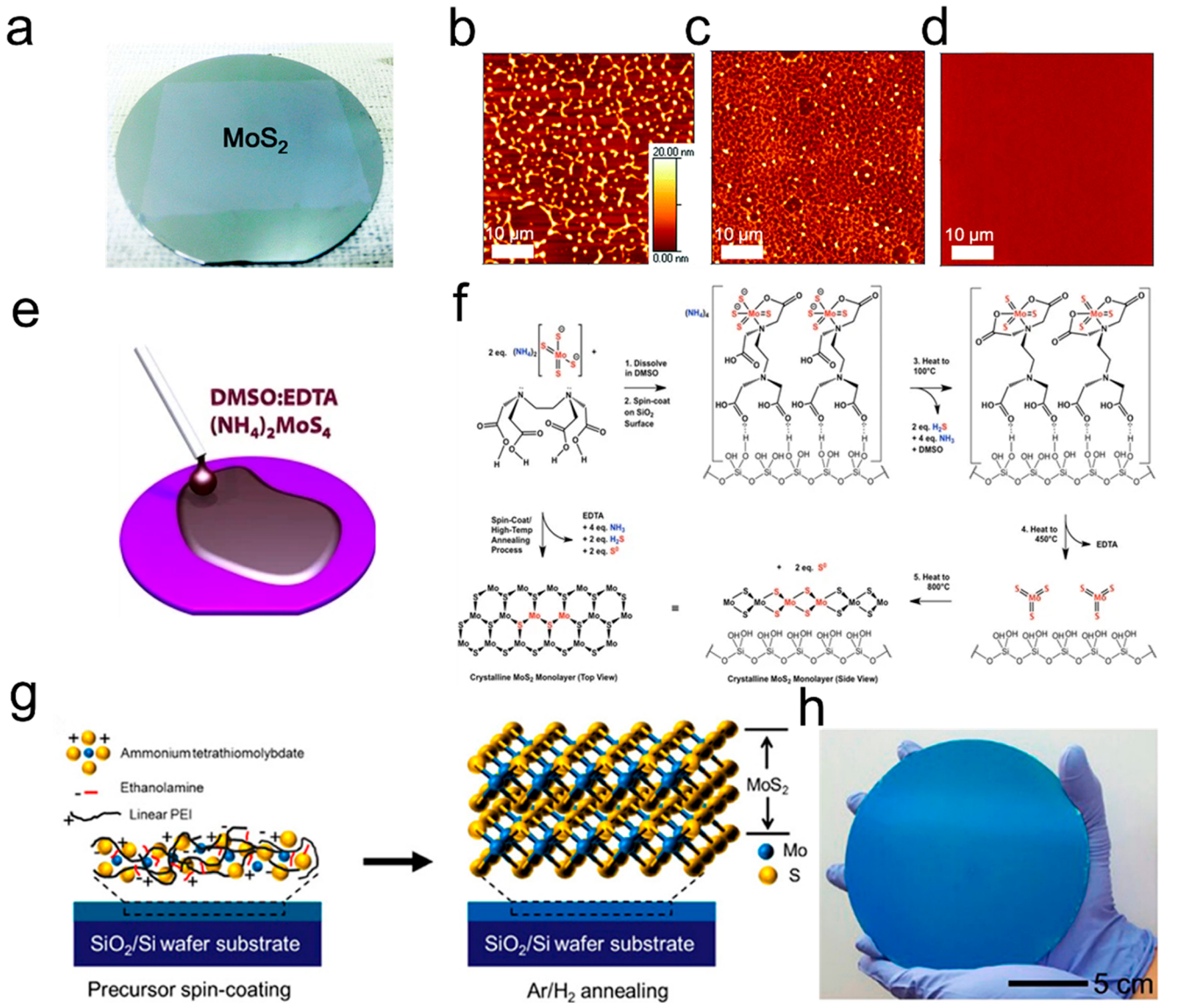

Figure 4. Synthesis of MoS_2 films using organic additives. (a) Optical image of a 2 in.-sized MoS_2 wafer thin film from SCVD using $(NH_4)_2MoS_4$-DMF solution with additional amine- and amino alcohol-based solvents (*n*-butylamine and 2-aminoethanol). (b–d) AFM images of the different spin-coated precursor films with additive of (b) only DMF, (c) DMF:2-aminoethanol, and (d) DMF:*n*-butylamine:2-aminoethanol. Reproduced from ref 54. Copyright 2015 Royal Society of Chemistry. (e) Schematic of wet behavior of solution of $(NH_4)_2MoS_4$-EDTA-DMSO. (f) Mechanism for the synthesis of MoS_2 crystal. Reproduced from ref 57. Copyright 2017 Springer Nature. (g) Schematic illustration of the formation of MoS_2 thin film from the anhydrous ammonium tetrathiopolybdate (ATM) precursor and linear polyimide (L-PEI) complex film. (h) Image of a 6 in.-sized MoS_2 thin film synthesized through the method illustrate in (g). Reproduced from ref 38. Copyright 2017 American Chemical Society.

Zhu et al. brought KOH (or NaOH) to the liquid-phase precursor to introduce −OH groups.[22] As illustrated in Figure 3a, −OH groups in solution aimed at attaching to the (001) surface of MoS_2 to form an S−Mo−S-OH bilayer structure during the growth process, which leads to preferential growth of MoS_2 layers in the lateral direction instead of in the vertical direction, further promoting the generation of large area monolayer MoS_2. The OM and AFM images in Figure 3b verified the uniform atomically flat MoS_2 film with a surface roughness of about 0.12 nm. Figure 3c shows representative uniform MoS_2 monolayers grown with 100% coverage on 1 × 1 and 3 × 3 cm^2 sapphire. Moreover, the test of devices fabricated from the obtained MoS_2 films suggested that the −OH layer on the monolayer MoS_2 surface could effectively suppress oxidation of MoS_2 in air, resulting in the highest carrier mobility up to 30 $cm^2\ V^{-1}\ s^{-1}$ in air. Hu et a reported a method for preparing nonfilter light storage transistors using a hydrophilic monolayer molybdenum disulfide film with strong charge trapping capability.[52] The hydroxyl groups covalently bonded with MoS_2 possess strong charge trapping capabilities, which can control the capture and release of electrons by laser and electric operation, thus achieving stable image memory functions, and promoting the development of artificial visual systems in the future. Furthermore, 1 × 1 cm^2 $MoTe_2$ monolayer can be grown using NaOH as additive (Figure 3d).[26] The spin-coated precursors, which can be dehydrated into immobilized particles during the reaction, were consumed continually to provide a source for the growth of the monolayer. The small roughness of 0.19 nm calculated from the AFM image in Figure 3e indicates the smoothness of the

https://doi.org/10.1021/prechem.3c00115
Precis. Chem. 2024, 2, 282−299

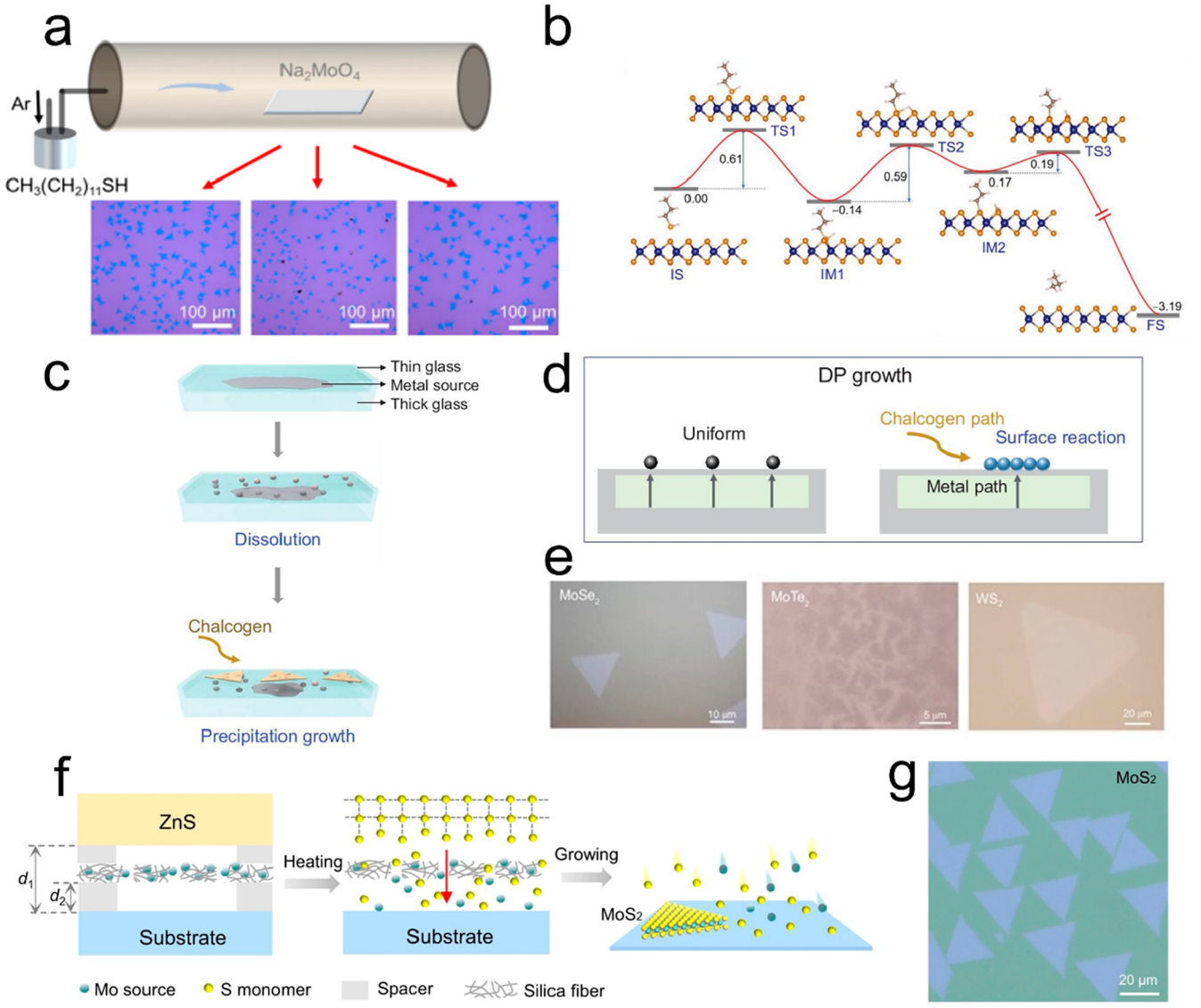

Figure 5. TMDs synthesized through new resource supply. (a) Schematic image of the bubbling setup and OM images of grown MoS_2 monolayers through the bubble method. (b) Simulation of in situ repairing process by thiol molecules. Reproduced from ref 36. Copyright 2020 John Wiley and Sons. (c) Illustration of the DP growth process. (d) Detail of DP growth during nucleation. (e) OM images of synthesized $MoSe_2$, $MoTe_2$, and WS_2 nanosheets through the DP method, respectively. Reproduced from ref 19. Copyright 2021 Oxford University Press. (f) Schematic model of sulfur (S) monomer supply for the growth of MoS_2. (g) OM image of the as-grown MoS_2 monolayers through monomer feeding method. Reproduced from ref 42. Copyright 2022 Springer Nature.

fabricated monolayer. The time-of-flight secondary ion mass spectrometry (ToF-SIMS) data in Figure 3f showed that −OH groups could be adsorbed on the surface of the $MoTe_2$ layer, which can inhibit the growth of $MoTe_2$ in the vertical direction. Ammonium salts have also been proved to be a clean and nondestructive additives for the synthesis of MoS_2.[53] Overall, the novel additives in the SCVD technique provide a new opportunity for the growth of inch-sized monolayer TMDs films, moving us closer to the realization of inch-scale functional nanomaterials.

Inorganic additives in the SCVD process for TMDs are multifaceted, acting not just as growth promoters but also as reducing and solubilizing agents. For example, Kim et al. incorporated hydrazine (N_2H_4) as a strong reducing agent into an aqueous Na_2WO_4 solution to prereduce Na_2WO_4 and facilitate the synthesis of WS_2.[43] The introduction of hydrazine into the reaction provides regulation over the synthesis, yielding a notable enhancement in the quality of the WS_2 product. The reduction of sodium tungstate by hydrazine generates enough volatile tungsten suboxides to directly participate in the growth of WS_2, avoiding the etching caused by H_2 reduction, thus ensuring the attainment of full coverage of the WS_2 film. Another method of forming a precursor solution is dissolving the oxide in an alkaline solvent.[34,41] Lee et al. reported the synthesis of MoS_2 monolayer with a size of up to 500 μm using the preprocessed solution composed of MoO_3 and NH_4OH.[41] However, the oxides dissolved in alkaline solvent as precursors are somewhat more complex in nature. Clearly, the role of inorganic additives during the SCVD growth of TMDs is versatile and extends beyond a singular function, underscoring their critical importance in

https://doi.org/10.1021/prechem.3c00115
Precis. Chem. 2024, 2, 282−299

tailoring and refining the quality and dimensions of the resulting materials.

Furthermore, organic additives such as dimethylformamide (DMF),[54,55] ethylene glycol,[56] and n-methylpyrollidone (NMP)[16] could be also used as effective agents for dissolving poorly water-soluble precursors. Theses precursors and the organic solvents can chemically bond to the precursor to form a stable solute in the mixture solution. Kim et al. utilized $(NH_4)_2MoS_4$-DMF solution with additional amine- and amino alcohol-based solvents (*n*-butylamine and 2-aminoethanol) to synthesize 2 in. wafer-scale MoS_2 thin films (Figure 4a).[54] As shown in Figure 4b−d, the spin-coated precursor film exhibits dewetted regions and pinholes when only DMF was used as solvent. After adding 2-aminoethanol to DMF, thiomolybdate clusters formed with a hydrogen bond with a hydroxide group, which enhanced the solubility of $(NH_4)_2MoS_4$. However, microsize defects still existed in this case. With the further addition of *n*-butylamine again, a defect-free spin-coating precursor film was finally obtained, and the 2 in. wafer-scale MoS_2 thin films were obtained in the following thermal process. Ozkan et al. used ethylenediaminetetraacetic acid (EDTA) and dimethyl sulfoxide (DMSO) as a solvent that dissolved $(NH_4)_2MoS_4$ to fabricate MoS_2 films (Figure 4e).[57] Figure 4f illustrates the mechanism for the synthesis of MoS_2 crystals through this strategy. Tetrathiomolybdate coordinates with EDTA, where the presence of both coordinated and uncoordinated carboxylic groups could enhance the interaction with the silanol-functionalized silica surface. Therefore, with EDTA and DMSO, the precursor solution can have superior wettability on the hydroxylated surface. Besides, Jeong et al. designed a precursor-polymer complex film consisting of anhydrous ammonium tetrathiopolybdate (ATM) precursor and linear polyimide (L-PEI) (Figure 4g,h),[38] which facilitates uniform coating of precursor on substrate over large areas and LPEI fully decomposes at 400 °C without residual carbon. From the above examples, it is evident that the utilization of organic additives can enhance the interaction of the precursors in the solution and enhance the wettability of the precursor on the substrate, thereby contributing to the synthesis of wafer-level TMDs film. However, while some organic additives can be decomposed without leaving residue, most of them still remain as contaminants and potentially compromise the quality of the crystal.

In summary, the strategic incorporation of the appropriate additives into precursor solutions in the SCVD process is remarkably beneficial. These additives can lower the melting point of the precursor, increase the vapor pressure, enable the formation of intermediates, reduce the activation energy, and increase the wettability of the precursor solution on substrate. Collectively, these effects synergistically contribute to the efficient synthesis of 2D TMDs.

2.1.3. Recent Advances in Developing the Source Supply Method. Not only will the metal or chalcogen source itself affect the material preparation but also the source supply method can affect the growth process. In recent years, new developed source supply methods such as bubble method, dissolution−precipitation method and monomer feeding method have introduced advanced capabilities in SCVD growth.[19,36,42,58] The supply of CH_3SSCH_3 and $C_{12}H_{25}SH$ precursor have been precisely controlled by bubble method during SCVD growth.[36,40] As Figure 5a shows, Liu et al. utilized bubbling suppling $C_{12}H_{25}SH$ as a continuous sulfur sources to react with Na_2MoO_4 during the synthesis of 2D MoS_2.[36] The synthesized MoS_2 crystals possess the lower density of sulfur vacancies (0.32 nm^{-2}) and the quality of that can even be close to that of exfoliated MoS_2. As simulated in Figure 5b, this is because thiol molecules could be chemically absorbed into the S vacancy to repair these defects in MoS_2. It offers a new idea to repair defects and decrease vacancies density in TMDs. Liu et al. reported the growth of uniform monolayer TMDs and their monolayer alloys, such as $MoSe_2$, WS_2, $MoTe_2$, and $Mo_xW_{1-x}S_2$, using the dissolution−precipitation (DP) method (Figure 5c−e).[19] The embedded metal source melted and diffused through the molten glass to its surface and reacted with chalcogen sources to attain TMDs. The soda lime glass acts as both a spin-coated substrate and metal source transferred layer, which achieves a uniform feed of the metal source while eliminating unwanted gas-phase reaction via independent diffusion path of the metal and chalcogen sources. On account of the inhibition of secondary nucleation by the DP method, the synthesized MoS_2 monolayers appear cleaner. Another strategy is to introduce an active chalcogen monomer supply.[42] As shown in Figure 5f (left panel), Zuo et al. put forward a stacked sandwiched model of ZnS, Na_2MoO_4 coated silica fiber fabric, mica spacer, and the substrate. When heated to growth temperature, the released S monomers from the ZnS and vaporized Na_2MoO_4 passed through the fiber fabric to form monolayer MoS_2 on the substrate (Figure 5f, right panel). Figure 5g shows the OM image of as-grown MoS_2. The density of sulfur vacancy defects in MoS_2 were measured as $\sim 2 \times 10^{12}$ cm^{-2} from STEM characterizations, which is among the lowest value of as-grown monolayer TMDs in previous literatures. Subsequently, a series of TMDs and alloys were synthesized in the same way by changing the transition metal sources (e.g., Na_2MoO_4 and Na_2WO_4) and chalcogenide plates (e.g., ZnS, ZnSe, and ZnTe). Moreover, Liu et al. produced a new bright spot in nonlinear optical fibers.[59]

The development of new source supply methods overcomes the uncontrollable nature of vaporization of solid metal and chalcogen precursors and therefore ensures the constant delivery of precursor vapors to the substrate surface. This steady delivery is essential for achieving uniformity and high quality in the synthesis of materials.

2.2. Substrate Engineering Strategies in SCVD Growth

The substrate plays a crucial role in the adsorption of source materials, promoting nucleation, and stimulating the epitaxial growth of nucleus during synthesis of 2D TMDs.[60] In the SCVD technique, various substrate engineering strategies have been developed to control nucleation, enhance growth, and improve the film quality. These strategies include careful selection of the substrate material, surface treatment, and substrate patterning.

2.2.1. Substrate Selection. Commonly used substrates in the SCVD technique include SiO_2/Si, sapphire, glass, and quartz. Given the requirements of SCVD growth, SiO_2/Si and sapphire stand out as the preferred substrate materials, meeting the specific requirements of growth of SCVD. The use of SiO_2/Si as a substrate for large-scale SCVD growth facilitates subsequent nanopatterning and integration and is highly compatible with metal-oxide-semiconductor (CMOS) technology. However, due to the amorphous surface of the SiO_2/Si substrate, the TMDs films grown on the SiO_2/Si are mostly polycrystalline with randomly oriented grains. The C-plane sapphire substrate, characterized by lattice symmetry that

https://doi.org/10.1021/prechem.3c00115
Precis. Chem. 2024, 2, 282−299

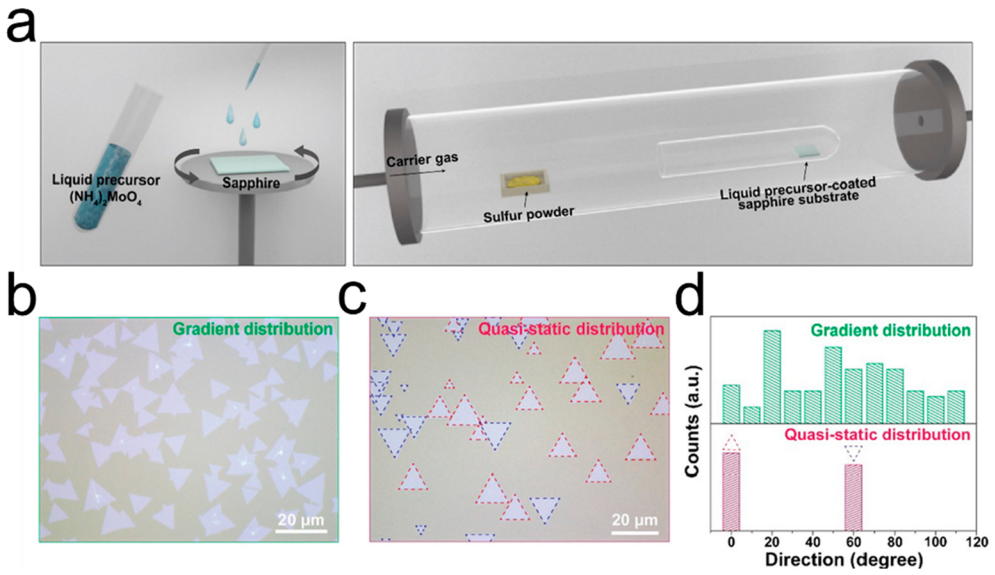

Figure 6. Well-aligned MoS_2 crystals on sapphire substrate. (a) Schematic illustration of controlling the chalcogen vapor pressure to grow MoS_2 on a sapphire substrate. (b–d) OM images (b,c) and the orientation histogram (d) of as-grown MoS_2 under gradient and quasi-static distributions of chalcogen vapor pressure. Reproduced from ref 29. Copyright 2021 American Chemical Society.

matches well with TMDs, proves to be more conducive for the growth of wafer-scale single crystal TMDs. Park group regulated chalcogen vapor pressure to guide MoS_2 seeds to grow along the preferred orientation of the lattice structure of the sapphire substrate, resulting in the well-aligned MoS_2 crystals (Figure 6a).[29] As shown in Figure 6b–d, the chalcogen atoms are inclined to low potential energy sites guided by the sapphire lattice structure, enabling the alignment of TMDs under an orientation of 0°/60°. Numerous studies[61−63] have demonstrated the crucial influence of substrates on the crystal orientation. It is expected to further investigate the impact of substrates on the orientation of TMDs in the SCVD technique.

2.2.2. Substrate Pretreatment Strategy. To ensure uniform deposition of precursors, substrates are typically pretreated using simple methods such as O_2 plasma,[18,42,64] piranha solution,[17,65] alkaline solution[39,40] and UV−O_3[66−68] to enhance hydrophilicity. These treatments improve the surface properties of the substrate and promote the adsorption of source materials, resulting in improved nucleation and growth of 2D TMDs.

For example, Figure 7 presents the OM of water contact angles on the SiO_2 surface and corresponding schematic illustration of the mechanism before and after O_2 plasma treatment.[64] After the O_2 plasma treatment, the SiO_2 surface becomes more hydrophilic. Oxygen plasma removes organic contaminants and breaks siloxane group (Si−O−Si) through chemical reactions with oxygen radicals, thus promoting the formation of Si−OH. That is, SiO_2 surface treated by oxygen plasma could form hydrogen bond with water molecules.[69] In particular, the water contact angles of the treated SiO_2 surface are 11.4°, which is lower than the water contact angle of the untreated SiO_2 surface of 45.2°, indicating an enhanced surface energy of the substrate. It is noteworthy that O_2 plasma treatment can not only eliminate natural contaminants on the surface of SiO_2, but also increase the surface energy, thereby improving the hydrophilicity. Moreover, Sodium cholate and iodixanol have been reported to function as a surfactant for increasing the wettability and viscosity of the aqueous precursor on the SiO_2/Si substrate.[21,70]

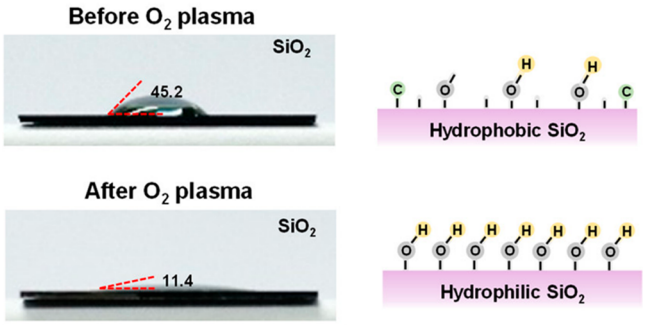

Figure 7. Optical images of the water contact angle on the SiO_2 surface and corresponding schematic illustrations before and after O_2 plasma treatment, respectively. Reproduced from ref 64. Copyright 2021 American Chemical Society.

2.2.3. Substrate Patterning. Precise patterned growth is crucial for the integration of functional materials into circuit devices but is difficult for the TMDs monolayers grown using typical CVD method due to the uncontrollable random nucleation seeds. While there have been reports of successful growth of patterned TMDs using predesigned Au, Cr, and Pt−Ti seeds, the complete removal of residual seeds remains exceedingly difficult, thereby limiting further research in this area.[71−73] People utilize micropipette tip, photolithography, and inkjet printing to pattern the substrate in the SCVD technique, enabling seed-free synthetic patterned TMDs. As is shown in Figure 8a, the strip patterned MoS_2 layers were obtained by dragging a precursor solution droplet via micropipette tip.[74] The droplet, dragged with variable velocities, induces an asymmetric shape as it moves across the substrate, resulting in spatial material deposition. It is well-known that lithography is an available patterning method.[51,64,75] Figure 8b shows arrays of MoS_2 nanoflakes grown from patterned Na_2MoO_4 squares. After arrays of square windows was fabricated on SiO_2/Si substrate by photolithography, the molybdenum-containing seed material was spin-coated with Na_2MoO_4 aqueous solution.[75] The seeds

https://doi.org/10.1021/prechem.3c00115
Precis. Chem. 2024, 2, 282−299

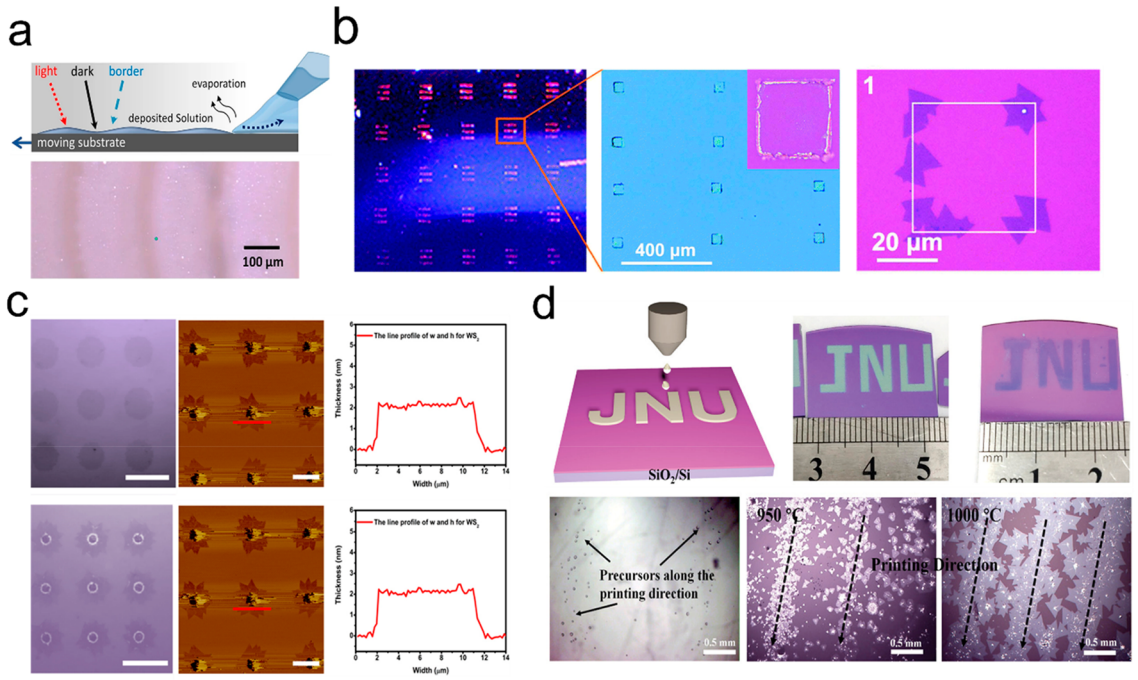

Figure 8. Synthesis of patterned TMDs via patterned substrate. (a) Schematic illustration and OM image of patterned MoS_2 layers by dragging a precursor solution droplet via micropipette tip. Reproduced from ref 74. Copyright 2021 Springer Nature. (b) Optical image of arrays of MoS_2 nanoflakes grown from patterned Na_2MoO_4 squares. Reproduced from ref 75. Copyright 2019 Royal Society of Chemistry. (c) OM and the corresponding atomic force microscope (AFM) images of patterned MoS_2 (upper) and WS_2 (bottom) nanoflakes via the DWP. Reproduced from ref 32. Copyright 2019 IOP Publishing Ltd. (d) Schematic model and OM images of monolayer "JNU" MoS_2 based on patterned aqueous precursors (upper) and the OM images of as-grown TMDs with different growth temperature along the printed aqueous precursors direction on the transparent glass substrate (bottom) via inkjet printing. Reproduced from ref 23. Copyright 2021 John Wiley and Sons.

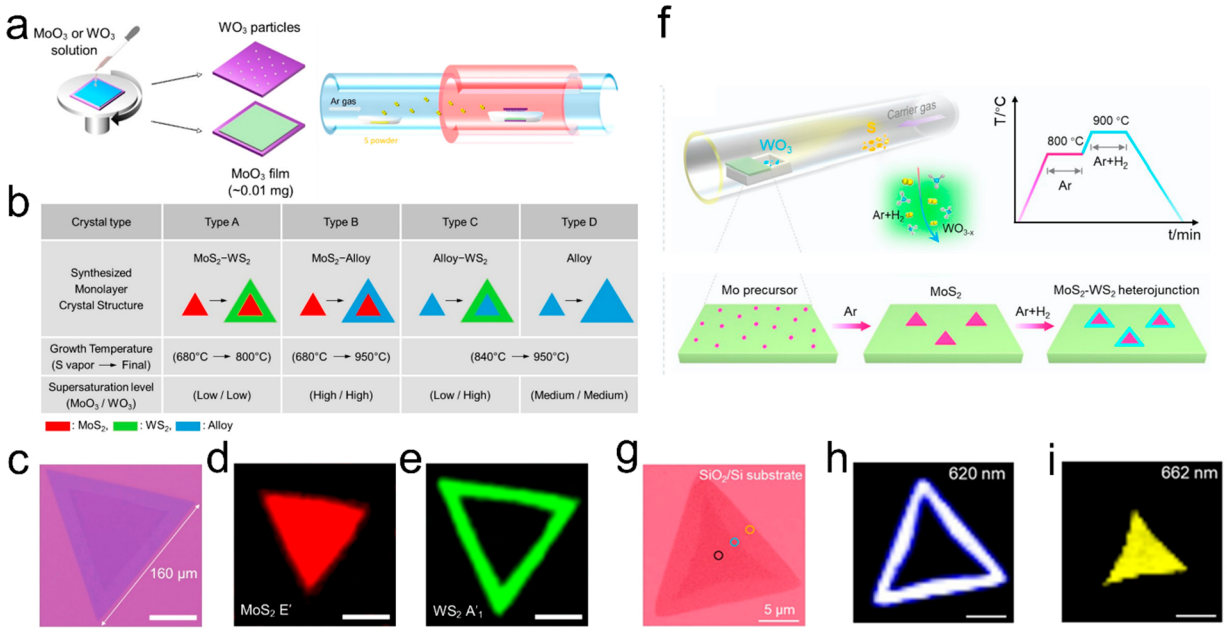

Figure 9. Synthesis of MoS_2–WS_2 lateral heterostructure with the SCVD strategy. (a) Growth process diagram of MoS_2–WS_2 lateral heterostructures and alloys. (b) Summary table of conditions for each monolayer structure. (c-e) OM image of a large sized typical MoS_2–WS_2 lateral heterostructure and the corresponding Raman mapping images of the E′ mode of MoS_2 and the A′1 mode of WS_2. Scale bar: 50 μm. Reproduced from ref 76. Copyright 2019 American Chemical Society. (f) Schematic diagram of MoS_2–WS_2 lateral heterostructure synthesized with hydrogen-triggered reaction. (g–i) OM image of MoS_2–WS_2 lateral heterostructure on SiO_2/Si substrate and the corresponding PL intensity mapping at 620 and 662 nm. Scale bar: 5 μm. Reproduced from ref 77. Copyright 2021 American Chemical Society.

accumulated at the edges of the patterned squares to form MoS_2 nanoflakes. However, it is obviously observed that the arrays of MoS_2 are not regular. Another mask-free approach seems simpler compared with photolithography. It is utilized to

https://doi.org/10.1021/prechem.3c00115
Precis. Chem. 2024, 2, 282–299

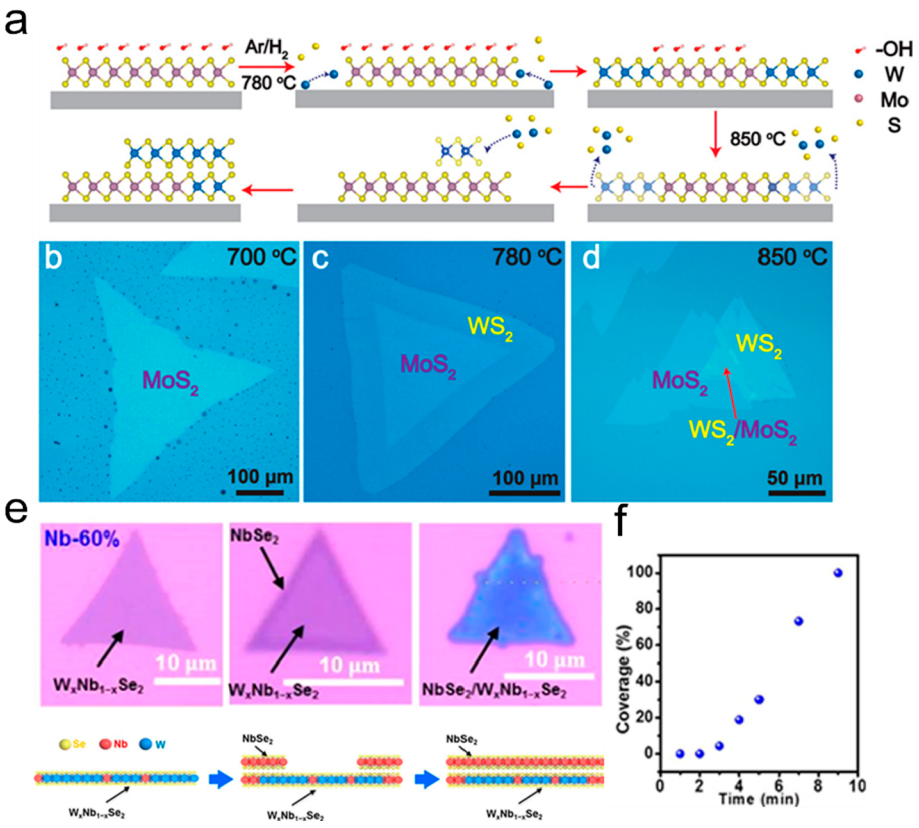

Figure 10. Synthesis of vertical heterostructures with SCVD strategy. (a) Schematic of the structural evolution of WS_2/MoS_2 heterostructures. (b–d) OM images of typical triangular MoS_2–OH and WS_2/MoS_2 lateral and vertical heterostructures. Reproduced from ref 79. Copyright 2020 American Chemical Society. (e) The Optical images and growth mechanism of $NbSe_2/W_xNb_{1-x}Se_2$ vdWHs (Nb-60%). (f) Coverage of $NbSe_2$ on the $W_xNb_{1-x}Se_2$ monolayer with growth time. Reproduced from ref 80. Copyright 2021 American Chemical Society.

deposit arrays of patterns on preselected locations via the direct write patterning (DWP) technique.[32] Figure 8c shows the representative images of grown patterned MoS_2 and WS_2 nanoflakes with a domain size of 8–10 μm and a thickness of average 2 nm. As for inkjet printing, it is supposed to be a desirable patterning way. The corresponding printed patterns in centimeter size like the word "JNU" were displayed in Figure 8d. When printed aqueous precursors along parallel direction began to melt, the inkjet-printed small nucleation centers appeared moving, coalescing, and merging with each other under maintaining the initial printing patterns.[23] However, further research is still needed to explore how to achieve high-precision control of precursors, enabling the preparation of single crystal patterns with high quality and industrial prospects.

Currently, the growth dynamics of 2D TMDs on substrates, particularly nucleation and growth processes aiming at wafer scale production of 2D TMDs, still need being explored. With the appropriate selection of substrates, modification of surface properties, or the utilization of prepatterned substrates, it is expected to gain more control over the nucleation and growth of 2D TMDs, ultimately enhancing film quality and achieving desired material properties.

3. NOVEL STRUCTURE OF TMDs OBTAINED BY SCVD

3.1. TMDs-Based Heterostructures

Combining different atomically thin transition metal dichalcogenides (TMDs) into vertically stacked or seamlessly connected planar structures can form van der Waals heterostructures (vdWHs) or lateral heterostructures. These heterostructures have significantly expanded the range of available material systems and provided a reliable platform for exploring novel physical and chemical properties, greatly broadening the application prospects of 2D TMDs. In recent developments, the SCVD growth method has been successfully applied in producing TMD heterostructures with large crystal sizes and clean interfaces.

Several studies have been reported on the successful synthesis of high-quality MoS_2–WS_2 lateral heterostructures using the SCVD method.[76−78] Kim et al. reported the preparation of various lateral heterostructures and alloys (WS_2–MoS_2, MoS_2-alloy, alloy-WS_2) (Figure 9a,b) by precisely adjusting growth parameters including the subsequent growth temperature, and the relative supersaturation level of MoO_3 and WO_3 precursors.[76] The MoO_3 and WO_3 precursor solutions were prepared by dissolving MoO_3 and WO_3 powders in NH_4OH. Following regular spin- coating treatment, the substrates containing MoO_3 film and WO_3 particles were positioned at the bottom and top of the crucible in the furnace, respectively (Figure 9a). Four types of as-grown monolayer lateral structures can be obtained: MoS_2/WS_2 heterostructures (type A), MoS_2/alloy heterostructures (type B), alloy/WS_2 heterostructures (type C), and alloy monolayer structures (type D) (Figure 9b). At low growth temperatures (~680 °C), due to the relatively high vaporization temperature of WO_3, there is almost no W precursor arrive the substrate coated with MoO_3, resulting in the formation of a single MoS_2 monolayer inside (referred to as type A and B). Upon heating

https://doi.org/10.1021/prechem.3c00115
Precis. Chem. 2024, 2, 282−299

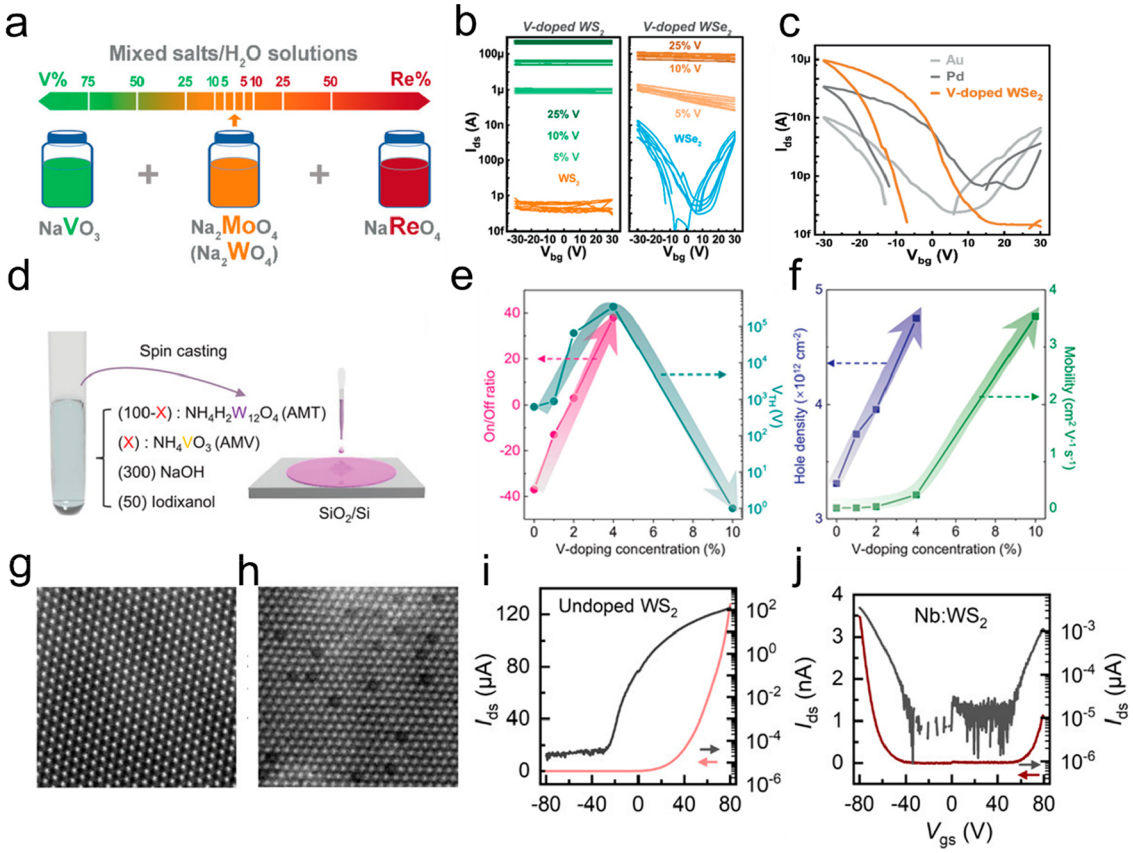

Figure 11. Synthesis of transition meatal doped TMDs. (a) Schematic illustration of preparing different ratios of mixed salt solutions for the fabrication of Re- and V-doped 2D TMDs. (b) Typical transfer curves of V-doped WS_2 and WSe_2 monolayers. (c) Transfer characteristics of WSe_2−FETs with three kinds of contacts including Au, Pd, and V-doped WSe_2. Reproduced from ref 68. Copyright 2021 John Wiley and Sons. (d) Schematic for preparation of V-doped WSe_2. (e,f) On/off ratio and threshold voltage (e), as well as the field-effect hole mobility and intrinsic hole carrier concentration (f), vary as a function of V-doping concentration. Reproduced from ref 82. Copyright 2020 John Wiley and Sons. (g,h) HAADF-STEM images of undoped (g) and doped (h) monolayer WS_2 crystals. Scale bars are 2 nm. (i,j) Transfer characteristics of undoped (i) and doped (j) monolayer WS_2 crystals. Reproduced from ref 65. Copyright 2019 American Chemical Society.

to ∼840 °C, both MoO_3 and WO_3 simultaneously vaporize and react with gaseous sulfur, leading to the formation of alloy-type monolayers in the core (referred to as types C and D). Then at the second growth step, at a low growth temperature of about 800 °C, WO_3 vaporize while MoO_3 do not, MoS_2/WS_2 lateral heterostructure with a clean interface (referred to as type A) can be synthesized. At higher growth temperatures of about 950 °C for the second growth step, alloy often appears at the interface of lateral heterostructure (referred to as type B and D) because MoO_3 violently vaporizes at high temperatures and coexists with the WO_3 precursor in the gas phase. Until MoO_3 is completely consumed, WS_2 will grow from the lateral side of the alloy monolayer, and a type C heterostructure can be formed. Figure 9c−e shows the OM images and the corresponding Raman mappings of the well-crystallized in-plane heterostructure consisting of MoS_2 monolayer inside and WS_2 outside. In another example, it is reported by Xu et al. that through H_2-triggered reaction, MoS_2−WS_2 lateral heterostructures with an ultraclean and defect-free narrow interface were synthesized.[77] Figure 9f schematically shows the two stages of the growth process. On the first stage, the MoS_2 monolayers were grown at 800 °C under pure Ar flow. Once exhausting Mo precursor completely, the H_2 was then introduced to trigger second growth of WS_2 at 900 °C. In fact, the sequential growth of MoS_2 and WS_2 is due to the different reaction conditions for the Mo-based precursor and the W-based precursor. Without H_2, only MoS_2 can grow on substrate. Under the presence of H_2, conversion of WO_3 to low-volatile W-based precursors happened and WS_2 can grow from the side of MoS_2. The typical OM image of the lateral MoS_2−WS_2 is shown in Figure 9f. The associated photoluminescence (PL) intensity mappings at 620 and 662 nm verified well the spatial distribution of MoS_2 and WS_2 domains (Figure 9g,h).

Changing the synthesis conditions to realize the sequential growth of varied materials is an important idea for synthesizing high quality vertical heterostructure with the SCVD method. Zhu et al. realized the optional growth of large WS_2/MoS_2 vertical heterostructures via hydroxide-assisted nucleation.[79] The agents KOH, $(NH_4)_2MoO_4$, and Na_2WO_4 were dissolved together in deionized water to obtain an aqueous solution containing −OH groups. Subsequently, the solution was spin-coated onto a clean sapphire substrate and then went through a three-stage growth process with sulfur atmospheres, resulting in vertical growth of WS_2/MoS_2. The specific reaction process and mechanism are described in Figure 10a. During the first stage, a large MoS_2−OH bilayer was obtained in an Ar + S atmosphere of about 700 °C. Figure 10b shows the OM image of a MoS_2−OH triangular domain with a length of about 600 μm. In the second stage, as the growth temperature was raised

https://doi.org/10.1021/prechem.3c00115
Precis. Chem. 2024, 2, 282−299

Table 3. Summary of Common Substitutionally Doped TMDs by the SCVD Technique

Dopant	Host	Precursor	Dopant type	Density (%)	References
P	WSe_2	$(NH_4)_6H_2W_{12}O_{40}{\cdot}4H_2O + P_2O_5 + Se$	p		91
V	MoS_2	$Na_2MoO_4 + NaVO_4 + S$	p	2.0∼6.0	90
	MoS_2	$(NH_4)_6Mo_7O_{24}{\cdot}4H_2O + NaVO_3 + S$	p	0.8−7.6	92
	MoS_2	$Na_2MoO_4 + NaVO_3 + S$	p	2.9	90
	WS_2	$Na_2WO_4 + NaVO_3 + S$		4.7	
	WSe_2	$Na_2WO_4 + NaVO_3 + Se$	p	2.7	
	WS_2	$(NH_4)_6H_2W_{12}O_{40}{\cdot}xH_2O + VO[SO_4] + S$	p	0.4−12	87
	WSe_2	$(NH_4)_6H_2W_{12}O_{40} + VO[SO_4] + Se$		0.5∼8	88
	WSe_2	$(NH_4)_6H_2W_{12}O_{40}{\cdot}xH_2O + NH_4VO_3 + Se$	p	0.1∼10	89
	WSe_2	$NH_4H_2W_{12}O_4 + NH_4VO_3 + Se$	p	1.0∼10	82
Cr	MoS_2	$Na_2MoO_4 + Na_2CrO_3 + S$			90
Fe	MoS_2	$Na_2MoO_4 + FeCl_3 + S$			90
	$MoSe_2$	$Na_2MoO_4 + FeCl_3{\cdot}6H_2O + Se$	n	0.93−6.10	93
	WS_2	$(NH_4)_6H_2W_{12}O_{40} + FeCl_3{\cdot}6H_2O + S$		0.7−2.8	70
Nb	WSe_2	$(NH_4)_6H_2W_{12}O_{40}{\cdot}xH_2O + C_4H_4NNbO_9{\cdot}xH2O + Se$	p	0.9∼9.1	21
	WS_2	$Na_2WO_4{\cdot}2H_2O + Nb(HC_2O_4)_5{\cdot}yH_2O + S$	p		65
Re	WS_2	$Na_2WO_4{\cdot}2H_2O + NaReO_4 + S$	n	1	83
	WS_2	$Na_2WO_4 + NaReO_4 + S$			68
	MoS_2	$Na_2MoO_4 + NaReO_4 + S$	n	2.1	
	WSe_2	$Na_2WO_4 + NaReO_4 + Se$			
	MoS_2	$(NH_4)_6Mo_7O_{24} + NaReO_4 + S$	n	0.3	70
Co	$MoSe_2$	$Na_2MoO_4 + CoCl_2{\cdot}6H_2O + Se$			93
Ni	$MoSe_2$	$Na_2MoO_4 + NiCl_2 + Se$			93
Yb/Er	WSe_2	$WO_3 + NaCl + Yb_2O_3/Er_2O_3$			84

to 780 °C in the S + Ar/H_2 mixed atmosphere, the growth of WS_2 was activated, promoting the lateral epitaxy of WS_2 on the MoS_2 edges under the protection of the −OH groups protection. Figure 10c presents the as-obtained WS_2−MoS_2 lateral heterostructures with a large lateral size of 700 μm. Finally, in the third stage, as the temperature continued to rise to 850 °C, the immediate decomposition of WS_2 and the OH− layer occurred, leading to the vertical nucleation of WS_2 on the MoS_2 surface and the formation of WS_2/MoS_2 vertical heterostructures (Figure 10d). Here, the numerous OH^- ions derived from KOH in the precursor solution are crucial for the selective growth of the desired heterostructure. Besides, the $NbSe_2/W_xNb_{1-x}Se_2$ vertical heterostructures has been successfully synthesized with $(NH_4)_6(H_2W_{12}O_{42}){\cdot}4H_2O$ and $C_4H_4NNbO_9{\cdot}xH_2O$ as W and Nb precursors.[80] As depicted in Figure 10e, at first the 2D $W_xNb_{1-x}Se_2$ domains formed; and when the reaction time increased, the Nb precursor continued to evaporate to preferentially nucleate at the edge of the as grown $W_xNb_{1-x}Se_2$ to form the $NbSe_2/W_xNb_{1-x}Se_2$ vertical heterostructures. Figure 10f shows the corresponding coverage of $NbSe_2$ on the $W_xNb_{1-x}Se_2$ monolayer with growth time.

Overall, 2D TMDs heterostructures provide a versatile platform for the integration of different materials with specific properties. To further broaden the applications of these materials, continued efforts are necessary to utilize SCVD technology to develop more extensive and various heterostructures.

3.2. Transition Metal Substitution of TMDs in SCVD

Compared with traditional CVD, the SCVD technique offers great flexibility in obtaining controllable transition metal (TM) doped TMDs. The utilization of mixed precursor solutions enables the tunability of doping concentrations for various dopants in different host materials, which resulting in tunable electrical,[65,68,80−82] optoelectrical,[83,84] catalytic[85,86] and magnetic[87−89] properties of TMDs beyond their intrinsic characteristics.

Recently, high-quality and tunable Re- and V-doped 2D TMDs[68] are synthesized using liquid precursor solutions ($NaReO_4$, $NaVO_3$, Na_2MoO_4, and Na_2WO_4) with controlled dopants molar ratio, as shown in Figure 11a. Figure 11b shows the typical FET transfer curves of V-doped WS_2 and WSe_2 monolayers. The V-doped WSe_2-contacted WSe_2 FETs has the high on-state current and on/off ratio than that of Au/Pd-contacted WSe_2 FETs in the Figure 11c, which indicated the SCVD grown V-doped WSe_2 monolayers could be as promising low-resistance electrode material for the p-type WSe_2 FETs. Such doping strategy is obvious convenient than doping through gas phase dopant, such as synthesis of Re-doped WSe_2 with precise control of the partial pressure of $Re_2(CO)_{10}$.[81] Similarly, Fan et al. used SCVD method to regulate the electrical properties of V-doped WSe_2 with different V doping concentration and thus realizing various band arrangements.[82] Figure 11d exhibits schematic for preparation of V-doped WSe_2 monolayers. The threshold voltage of the V-doped WSe_2 monolayer shifted to a positive value and showed obvious p-type transport characteristics (Figure 11e), and the hole mobility and carrier density increased with the increase of V doping concentration (Figure 11f). Additionally, Vu et al. precisely manipulated the ratio of Nb/(W + Nb) in the solution to control the hole carrier concentration and the corresponding contact resistance R_C value.[80]

In another example, different proportions of $Na_2WO_4{\cdot}2H_2O$ and $Nb(HC_2O_4)_5{\cdot}yH_2O$ mixed solutions were spin-coated on the SiO_2/Si to obtain Nb-doped WS_2 nanosheets with different Nb concentrations.[65] The STEM images reveal that 10.3% Nb-doped WS_2 exhibited darker spots at the W atom position compared to the undoped WS_2 (Figure 11g,h), confirming the random in situ atomic substitution of Nb doping. Furthermore,

https://doi.org/10.1021/prechem.3c00115
Precis. Chem. 2024, 2, 282−299

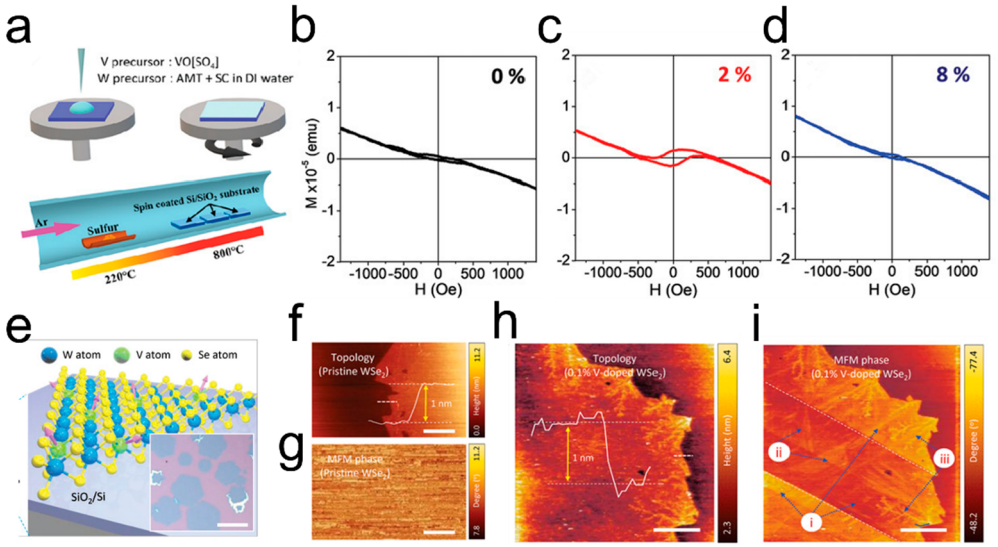

Figure 12. Synthesis of transition meatal doped TMDs. (a) Schematic of synthetic process of V-doped WS_2 monolayers. (b–d) Magnetization versus field loops of V-doped WS_2 monolayers at 0, 2, and 8 atom % at 300 K. Reproduced from ref 87. Copyright 2020 John Wiley and Sons. (e) Schematic of fabricated V-doped WSe_2 monolayers. The inset shows an optical image of SCVD-grown V-doped WSe_2 monolayer. Scale bar, 50 μm. (f,g) Topography and MFM phase images of pristine WSe_2 at room temperature, respectively. (h,i) Topography and MFM phase images of 0.1% V-doped WSe_2 at room temperature, respectively. Reproduced from ref 89. Copyright 2020 John Wiley and Sons.

the FETs based on 10.3% Nb-doped WS_2 displayed clear indications of hole doping, while the undoped WS_2 FETs exhibited n-type behavior (Figure 11 i,j), providing evidence that the Nb dopant acts as a p-type dopant. Additionally, V-doped MoS_2 and Nb-doped WS_2 nanosheets displayed p-type conductivity,[65,90] whereas Re-doped MoS_2 presented n-type behavior.[68] In addition to the tunable electrical properties, there have also been reports of changes in optical properties. Zhang et al. continuously increased the proportion of Nb components in the $Nb_{1-X}W_XSe_2$ alloy to realize the continuous shift of PL peak from 760 to 845 nm.[48] The Nb atoms act as electron acceptors in the WSe_2, resulting in a change of the energy band gap. Eda et al. observed a well-defined impurity-induced emission in Re-doped WS_2 monolayers as neutral donors.[83] Gao et al. realized a fascinating up-converted luminescence on the Yb–Er codoped bilayer WSe_2 excited by 980 nm laser.[84] A series of experimental reports on as-grown doped-TMDs using the SCVD technique is summarized in Table 3.

Apart from altering the electrical properties of 2D TMDs, the incorporation of suitable doping atoms into the host can also change the magnetic properties of these materials. Both theoretical and experimental reseach have indicated that doping with transition metal elements such as Cr, Mn, Fe, and Co can enable the realization of ferromagnetism in inherently nonferromagnetic TMDs.[94−99] The SCVD technique has been proven to be an effective and straightforward method for the controlled synthesis of dilute magnetic semiconductors (DMSs). V doping is one of the common magnetic doping.[87,89] Zhang et al. prepared V-doped WS_2 monolayers with V concentration ranges from 0 to 12% to obtain room-temperature ferromagnetic order.[87] Figure 12a shows a schematic of the synthetic process of V-doped WS_2 monolayers. Figure 12b–d depicts the relationship between ferromagnetism and the V doping concentration at room temperature. It can be seen that, with the increase of V doping concentration, the ferromagnetic intensity of V-doped WS_2 increases. Specifically, when the concentration of V doping in WS_2 reaches 2%, the coercivity and saturation magnetization of the material reach their maximum values, which is also applied in the WSe_2 host. Yun et al. reported V-doped WSe_2 monolayer induces long-range ferromagnetism at room temperature. The OM image of V-doped WSe_2 monolayers is shown in Figure 12e. Figure 12f,g shows topography and MFM phase images of pristine WSe_2 at room temperature.[89] With the increasing V concentration from 0.5 to 8 atom % WSe_2, the magnetization gradually realized the enhancement. Figure 12h,i exhibits the existence of the ferromagnetic order from the microscopic scale of magnetic force microscopy (MFM). And the ferromagnetic enhancement of the V-doped WSe_2 monolayer has been achieved by adjusting the complex Se vacancies structure through post heat-treatment.[100] In addition to V atoms, Fe, Co and Ni has been successfully doped into $MoSe_2$ using the SCVD technique to modulate the magnetism.[93]

4. CONCLUSIONS AND PERSPECTIVES

In summary, we discussed recent advancements in the growth of 2D TMDs using the SCVD technique. A variety of liquid precursors, additives, and new source supply methods for the synthesis of larger area and higher quality monolayer TMDs, even wafer-level homogeneous films, are reviewed. Substrate engineering strategies, including selection of the substrate, surface treatment, and substrate patterning, are studied to precisely control the nucleation and growth of TMD films. In addition, we provide an overview of the latest progress in the SCVD growth of 2D TMDs heterostructures and 2D doped TMDs. Despite these advancements, challenges still exist in the SCVD technique, and it is important to address these challenges to explore new synthesis method of 2D TMD with wafer scale area, high crystal quality, high reproductivity, and low cost:

(I) The SCVD technique offers numerous opportunities for synthesizing atomically thin and high-quality 2D TMDs.

https://doi.org/10.1021/prechem.3c00115
Precis. Chem. 2024, 2, 282−299

Further research should focus on finding more novel liquid precursors or utilizing additives which could increase the solubility of precursors to expand the materials library. Additionally, exploring the growth of ternary or multielement 2D materials by mixing multiple precursors could be a promising direction.

(II) In view of the fact that monolayer MoS_2 and WS_2 single crystal films have been successfully achieved on single-crystal Au substrates and well-designed sapphire substrates, it seems to be a feasible approach to explore new or pretreated growth substrates that have good contact with precursor solutions, and then seamlessly grow and link unidirectional domains into wafer-level single crystal films by inhibiting nucleation rate and promoting edge-induced growth.

(III) The development of patterned growth of TMDs using substrate patterning in the SCVD technique has shown many superiorities. However, there is still a need to realize large-area with well-controllable size and morphology arrays for the application in integrated circuits. Further advancements in patterning techniques will be crucial for enabling the practical implementation of TMD-based devices.

(IV) More in-depth studies on doped/alloyed 2D TMDs are necessary. Controlling the doping concentrations and defect density of doped TMDs is crucial as it can effectively regulate the electrical and optical properties of TMDs. Further research efforts should be dedicated to understanding and optimizing the doping processes to unlock the full potential of doped TMDs in various applications.

AUTHOR INFORMATION

Corresponding Authors

Xidong Duan − *Hunan Key Laboratory of Two-Dimensional Materials, State Key Laboratory for Chemo/Biosensing and Chemometrics, College of Chemistry and Chemical Engineering, Hunan University, 410082 Changsha, China;* orcid.org/0000-0002-4951-901X; Email: xidongduan@hnu.edu.cn

Bei Zhao − *Key Laboratory of Quantum Materials and Devices of Ministry of Education, School of Physics, Southeast University, Nanjing 211189, China*; Email: beizhao@seu.edu.cn

Authors

Dingyi Shen − *Hunan Key Laboratory of Two-Dimensional Materials, State Key Laboratory for Chemo/Biosensing and Chemometrics, College of Chemistry and Chemical Engineering, Hunan University, 410082 Changsha, China*

Yejun Jin − *Hunan Key Laboratory of Two-Dimensional Materials, State Key Laboratory for Chemo/Biosensing and Chemometrics, College of Chemistry and Chemical Engineering, Hunan University, 410082 Changsha, China*

Zucheng Zhang − *Hunan Key Laboratory of Two-Dimensional Materials, State Key Laboratory for Chemo/Biosensing and Chemometrics, College of Chemistry and Chemical Engineering, Hunan University, 410082 Changsha, China*

Rong Song − *Hunan Key Laboratory of Two-Dimensional Materials, State Key Laboratory for Chemo/Biosensing and Chemometrics, College of Chemistry and Chemical Engineering, Hunan University, 410082 Changsha, China*

Miaomiao Liu − *Hunan Key Laboratory of Two-Dimensional Materials, State Key Laboratory for Chemo/Biosensing and Chemometrics, College of Chemistry and Chemical Engineering, Hunan University, 410082 Changsha, China*

Wei Li − *Hunan Key Laboratory of Two-Dimensional Materials, State Key Laboratory for Chemo/Biosensing and Chemometrics, College of Chemistry and Chemical Engineering, Hunan University, 410082 Changsha, China*

Xin Li − *Hunan Key Laboratory of Two-Dimensional Materials, State Key Laboratory for Chemo/Biosensing and Chemometrics, College of Chemistry and Chemical Engineering, Hunan University, 410082 Changsha, China*

Ruixia Wu − *Hunan Key Laboratory of Two-Dimensional Materials, State Key Laboratory for Chemo/Biosensing and Chemometrics, College of Chemistry and Chemical Engineering, Hunan University, 410082 Changsha, China*

Bo Li − *School of Physics and Electronics, Hunan University, 410082 Changsha, China;* orcid.org/0000-0002-5802-7519

Jia Li − *Hunan Key Laboratory of Two-Dimensional Materials, State Key Laboratory for Chemo/Biosensing and Chemometrics, College of Chemistry and Chemical Engineering, Hunan University, 410082 Changsha, China*

Complete contact information is available at: https://pubs.acs.org/10.1021/prechem.3c00115

Author Contributions

‡D.S. and Y.J. contributed equally.

Notes

The authors declare no competing financial interest.

ACKNOWLEDGMENTS

We acknowledge the support from the National Key R&D Program of the Ministry of Science and Technology of China (No. 2022YFA1203801), the National Natural Science Foundation of China (grant numbers 51991340, 51991343, 52221001, 62205055), the Hunan Key R&D Program Project (No. 2022GK2005), and Natural Science Foundation of Jiangsu Province (BK20220860).

REFERENCES

(1) Novoselov, K. S.; Geim, A. K.; Morozov, S. V.; Jiang, D.; Zhang, Y.; Dubonos, S. V.; Grigorieva, I. V.; Firsov, A. A. Electric Field Effect in Atomically Thin Carbon Films. *Science* **2004**, *306* (696), 666−669.

(2) Duan, X.; Wang, C.; Pan, A.; Yu, R.; Duan, X. Two-Dimensional Transition Metal Dichalcogenides as Atomically Thin Semiconductors: Opportunities and Challenges. *Chem. Soc. Rev.* **2015**, *44* (24), 8859−8876.

(3) Ovchinnikov, D.; Allain, A.; Huang, Y. S.; Dumcenco, D.; Kis, A. Electrical Transport Properties of Single-Layer WS_2. *ACS Nano* **2014**, *8* (8), 8174−8181.

(4) Lee, C. H.; Lee, G. H.; van der Zande, A. M.; Chen, W.; Li, Y.; Han, M.; Cui, X.; Arefe, G.; Nuckolls, C.; Heinz, T. F.; Guo, J.; Hone, J.; Kim, P. Atomically Thin p-n Junctions with van der Waals Heterointerfaces. *Nat. Nanotechnol.* **2014**, *9* (9), 676−681.

(5) Migliato Marega, G.; Zhao, Y.; Avsar, A.; Wang, Z.; Tripathi, M.; Radenovic, A.; Kis, A. Logic-In-Memory Based on An Atomically Thin Semiconductor. *Nature* **2020**, *587* (7832), 72−77.

(6) Sangwan, V. K.; Lee, H. S.; Bergeron, H.; Balla, I.; Beck, M. E.; Chen, K. S.; Hersam, M. C. Multi-Terminal Memtransistors from

Polycrystalline Monolayer Molybdenum Disulfide. *Nature* **2018**, *554* (7693), 500−504.
(7) Bonaccorso, F.; Colombo, L.; Yu, G.; Stoller, M.; Tozzini, V.; Ferrari, A. C.; Ruoff, R. S.; Pellegrini, V. 2D materials. Graphene, related two-dimensional crystals, and hybrid systems for energy conversion and storage. *Science* **2015**, *347* (6217), 1246501.
(8) Waldrop, M. M. More than moore. *Nature* **2016**, *530* (7589), 144−148.
(9) Liu, Y.; Duan, X.; Shin, H. J.; Park, S.; Huang, Y.; Duan, X. Promises and prospects of two-dimensional transistors. *Nature* **2021**, *591* (7848), 43−53.
(10) Cao, W.; Bu, H.; Vinet, M.; Cao, M.; Takagi, S.; Hwang, S.; Ghani, T.; Banerjee, K. The future transistors. *Nature* **2023**, *620* (7974), 501−515.
(11) Zhou, J.; Lin, J.; Huang, X.; Zhou, Y.; Chen, Y.; Xia, J.; Wang, H.; Xie, Y.; Yu, H.; Lei, J.; Wu, D.; Liu, F.; Fu, Q.; Zeng, Q.; Hsu, C. H.; Yang, C.; Lu, L.; Yu, T.; Shen, Z.; Lin, H.; Yakobson, B. I.; Liu, Q.; Suenaga, K.; Liu, G.; Liu, Z. A library of atomically thin metal chalcogenides. *Nature* **2018**, *556* (7701), 355−359.
(12) Li, S.; Wang, S.; Tang, D.-M.; Zhao, W.; Xu, H.; Chu, L.; Bando, Y.; Golberg, D.; Eda, G. Halide-assisted atmospheric pressure growth of large WSe_2 and WS_2 monolayer crystals. *Applied Materials Today* **2015**, *1* (1), 60−66.
(13) Zhang, K.; Bersch, B. M.; Zhang, F.; Briggs, N. C.; Subramanian, S.; Xu, K.; Chubarov, M.; Wang, K.; Lerach, J. O.; Redwing, J. M.; Fullerton-Shirey, S. K.; Terrones, M.; Robinson, J. A. Considerations for Utilizing Sodium Chloride in Epitaxial Molybdenum Disulfide. *ACS Applied Mater. Interfaces* **2018**, *10* (47), 40831−40837.
(14) Fang, H.; Tosun, M.; Seol, G.; Chang, T. C.; Takei, K.; Guo, J.; Javey, A. Degenerate n-doping of few-layer transition metal dichalcogenides by potassium. *Nano Lett.* **2013**, *13* (5), 1991−1995.
(15) Yun, S. J.; Chae, S. H.; Kim, H.; Park, J. C.; Park, J. H.; Han, G. H.; Lee, J. S.; Kim, S. M.; Oh, H. M.; Seok, J.; Jeong, M. S.; Kim, K. K.; Lee, Y. H. Synthesis of Centimeter-Scale Monolayer Tungsten Disulfide Film on Gold Foils. *ACS Nano* **2015**, *9* (5), 5510−5519.
(16) George, A. S.; Mutlu, Z.; Ionescu, R.; Wu, R. J.; Jeong, J. S.; Bay, H. H.; Chai, Y.; Mkhoyan, K. A.; Ozkan, M.; Ozkan, C. S. Wafer Scale Synthesis and High Resolution Structural Characterization of Atomically Thin MoS_2 Layers. *Adv. Funct. Mater.* **2014**, *24* (47), 7461−7466.
(17) Liu, K. K.; Zhang, W.; Lee, Y. H.; Lin, Y. C.; Chang, M. T.; Su, C. Y.; Chang, C. S.; Li, H.; Shi, Y.; Zhang, H.; Lai, C. S.; Li, L. J. Growth of large-area and highly crystalline MoS_2 thin layers on insulating substrates. *Nano Lett.* **2012**, *12* (3), 1538−1544.
(18) Liu, H.; Qi, G.; Tang, C.; Chen, M.; Chen, Y.; Shu, Z.; Xiang, H.; Jin, Y.; Wang, S.; Li, H.; Ouzounian, M.; Hu, T. S.; Duan, H.; Li, S.; Han, Z.; Liu, S. Growth of Large-Area Homogeneous Monolayer Transition-Metal Disulfides via a Molten Liquid Intermediate Process. *ACS Applied Mater. Interfaces* **2020**, *12* (11), 13174−13181.
(19) Cai, Z.; Lai, Y.; Zhao, S.; Zhang, R.; Tan, J.; Feng, S.; Zou, J.; Tang, L.; Lin, J.; Liu, B.; Cheng, H. M. Dissolution-precipitation growth of uniform and clean two dimensional transition metal dichalcogenides. *National Science Review* **2021**, *8* (3), nwaa115.
(20) Li, S.; Lin, Y.-C.; Hong, J.; Gao, B.; Lim, H. E.; Yang, X.; Liu, S.; Tateyama, Y.; Tsukagoshi, K.; Sakuma, Y.; Suenaga, K.; Taniguchi, T. Mixed-Salt Enhanced Chemical Vapor Deposition of Two-Dimensional Transition Metal Dichalcogenides. *Chem. Mater.* **2021**, *33* (18), 7301−7308.
(21) Park, S.; Yun, S. J.; Kim, Y. I.; Kim, J. H.; Kim, Y. M.; Kim, K. K.; Lee, Y. H. Tailoring Domain Morphology in Monolayer $NbSe_2$ and $W_xNb_{1-x}Se_2$ Heterostructure. *ACS Nano* **2020**, *14* (7), 8784−8792.
(22) Zhu, J.; Xu, H.; Zou, G.; Zhang, W.; Chai, R.; Choi, J.; Wu, J.; Liu, H.; Shen, G.; Fan, H. MoS2-OH Bilayer-Mediated Growth of Inch-Sized Monolayer MoS_2 on Arbitrary Substrates. *J. Am. Chem. Soc.* **2019**, *141* (13), 5392−5401.
(23) Wan, X.; Miao, X.; Yao, J.; Wang, S.; Shao, F.; Xiao, S.; Zhan, R.; Chen, K.; Zeng, X.; Gu, X.; Xu, J. In Situ Ultrafast and Patterned Growth of Transition Metal Dichalcogenides from Inkjet-Printed Aqueous Precursors. *Adv. Mater.* **2021**, *33* (16), e2100260.
(24) Kim, M.; Seo, J.; Kim, J.; Moon, J. S.; Lee, J.; Kim, J. H.; Kang, J.; Park, H. High-Crystalline Monolayer Transition Metal Dichalcogenides Films for Wafer-Scale Electronics. *ACS Nano* **2021**, *15* (2), 3038−3046.
(25) Chen, K.; Wan, X.; Xie, W.; Wen, J.; Kang, Z.; Zeng, X.; Chen, H.; Xu, J. Lateral Built-In Potential of Monolayer MoS_2-WS_2 In-Plane Heterostructures by a Shortcut Growth Strategy. *Adv. Mater.* **2015**, *27* (41), 6431−6437.
(26) Ma, L.; Zhu, J.; Li, W.; Huang, R.; Wang, X.; Guo, J.; Choi, J. H.; Lou, Y.; Wang, D.; Zou, G. Immobilized Precursor Particle Driven Growth of Centimeter-Sized $MoTe_2$ Monolayer. *J. Am. Chem. Soc.* **2021**, *143* (33), 13314−13324.
(27) Naylor, C. H.; Parkin, W. M.; Ping, J.; Gao, Z.; Zhou, Y. R.; Kim, Y.; Streller, F.; Carpick, R. W.; Rappe, A. M.; Drndic, M.; Kikkawa, J. M.; Johnson, A. T. Monolayer Single-Crystal 1T'-$MoTe_2$ Grown by Chemical Vapor Deposition Exhibits Weak Antilocalization Effect. *Nano Lett.* **2016**, *16* (7), 4297−4304.
(28) Naylor, C. H.; Parkin, W. M.; Gao, Z.; Kang, H.; Noyan, M.; Wexler, R. B.; Tan, L. Z.; Kim, Y.; Kehayias, C. E.; Streller, F.; Zhou, Y. R.; Carpick, R.; Luo, Z.; Park, Y. W.; Rappe, A. M.; Drndic, M.; Kikkawa, J. M.; Johnson, A. T. C. Large-area synthesis of high-quality monolayer 1T'-WTe_2 flakes. *2D Materials* **2017**, *4* (2), 021008.
(29) Seo, J.; Lee, J.; Baek, S.; Jung, W.; Oh, N. K.; Son, E.; Park, H. Liquid Precursor-Mediated Epitaxial Growth of Highly Oriented 2D van der Waals Semiconductors toward High-Performance Electronics. *ACS Applied Electronic Materials* **2021**, *3* (12), 5528−5536.
(30) Zhao, C.; Meng, C.; Wang, B.; Wang, C.; Li, R.; Fu, Q. Vapor−Liquid−Solid Growth of Thin and Epitaxial Transition Metal Nitride Nanosheets for Catalysis and Energy Conversion. *ACS Applied Nano Materials* **2021**, *4* (10), 10735−10742.
(31) Wang, B.; Zhao, C.; Wang, C.; Li, R.; Zhang, G.; Mu, R.; Fu, Q. Low-temperature growth of ultrathin and epitaxial Mo_2C nanosheets via a vapor-liquid-solid process. *Nanoscale* **2022**, *14* (25), 9142−9149.
(32) Alameri, D.; Nasr, J. R.; Karbach, D.; Liu, Y.; Divan, R.; Das, S.; Kuljanishvili, I. Mask-free patterning and selective CVD-growth of 2D-TMDCs semiconductors. *Semicond. Sci. Technol.* **2019**, *34* (8), 085010.
(33) Wang, S.; Zhang, Y.; Zhao, D.; Li, J.; Kang, H.; Zhao, S.; Jin, T.; Zhang, J.; Xue, Z.; Wang, Y.; Sui, Y.; Chen, Z.; Peng, S.; Jin, Z.; Liu, X.; Wang, J.; Chen, Y.; Yu, G. Fast and controllable synthesis of AB-stacked bilayer MoS_2 for photoelectric detection. *2D Materials* **2022**, *9* (1), 015016.
(34) Lu, Y.; Chen, T.; Ryu, G. H.; Huang, H.; Sheng, Y.; Chang, R. J.; Warner, J. H. Self-Limiting Growth of High-Quality 2D Monolayer MoS_2 by Direct Sulfurization Using Precursor-Soluble Substrates for Advanced Field-Effect Transistors and Photodetectors. *ACS Applied Nano Materials* **2019**, *2* (1), 369−378.
(35) Khan, H.; Medina, H.; Tan, L. K.; Tjiu, W.; Boden, S. A.; Teng, J.; Nandhakumar, I. A Single-Step Route to Single-Crystal Molybdenum Disulphide (MoS_2) Monolayer domains. *Sci. Rep.* **2019**, *9* (1), 4142.
(36) Feng, S.; Tan, J.; Zhao, S.; Zhang, S.; Khan, U.; Tang, L.; Zou, X.; Lin, J.; Cheng, H. M.; Liu, B. Synthesis of Ultrahigh-Quality Monolayer Molybdenum Disulfide through In Situ Defect Healing with Thiol Molecules. *Small* **2020**, *16* (35), e2003357.
(37) Ji, Q.; Su, C.; Mao, N.; Tian, X.; Idrobo, J. C.; Miao, J.; Tisdale, W. A.; Zettl, A.; Li, J.; Kong, J. Revealing the Brønsted-Evans-Polanyi relation in halide-activated fast MoS_2 growth toward millimeter-sized 2D crystals. *Science. Advances* **2021**, *7* (44), eabj3274.
(38) Yang, H.; Giri, A.; Moon, S.; Shin, S.; Myoung, J.-M.; Jeong, U. Highly Scalable Synthesis of MoS_2 Thin Films with Precise Thickness Control via Polymer-Assisted Deposition. *Chem. Mater.* **2017**, *29* (14), 5772−5776.
(39) Cun, H.; Macha, M.; Kim, H.; Liu, K.; Zhao, Y.; LaGrange, T.; Kis, A.; Radenovic, A. Wafer-scale MOCVD growth of monolayer MoS_2 on sapphire and SiO_2. *Nano Research* **2019**, *12* (10), 2646−2652.

https://doi.org/10.1021/prechem.3c00115
Precis. Chem. 2024, 2, 282−299

(40) Boandoh, S.; Choi, S. H.; Park, J. H.; Park, S. Y.; Bang, S.; Jeong, M. S.; Lee, J. S.; Kim, H. J.; Yang, W.; Choi, J. Y.; Kim, S. M.; Kim, K. K. A Novel and Facile Route to Synthesize Atomic-Layered MoS_2 Film for Large-Area Electronics. *Small* **2017**, *13* (39), 1701306.
(41) Lee, J.; Pak, S.; Giraud, P.; Lee, Y. W.; Cho, Y.; Hong, J.; Jang, A. R.; Chung, H. S.; Hong, W. K.; Jeong, H. Y.; Shin, H. S.; Occhipinti, L. G.; Morris, S. M.; Cha, S.; Sohn, J. I.; Kim, J. M. Thermodynamically Stable Synthesis of Large-Scale and Highly Crystalline Transition Metal Dichalcogenide Monolayers and their Unipolar n-n Heterojunction Devices. *Adv. Mater.* **2017**, *29* (33), 1702206.
(42) Zuo, Y.; Liu, C.; Ding, L.; Qiao, R.; Tian, J.; Liu, C.; Wang, Q.; Xue, G.; You, Y.; Guo, Q.; Wang, J.; Fu, Y.; Liu, K.; Zhou, X.; Hong, H.; Wu, M.; Lu, X.; Yang, R.; Zhang, G.; Yu, D.; Wang, E.; Bai, X.; Ding, F.; Liu, K. Robust growth of two-dimensional metal dichalcogenides and their alloys by active chalcogen monomer supply. *Nat. Commun.* **2022**, *13* (1), 1007.
(43) Choi, S. H.; Boandoh, S.; Lee, Y. H.; Lee, J. S.; Park, J. H.; Kim, S. M.; Yang, W.; Kim, K. K. Synthesis of Large-Area Tungsten Disulfide Films on Pre-Reduced Tungsten Suboxide Substrates. *ACS Applied Mater. Interfaces* **2017**, *9* (49), 43021−43029.
(44) Pace, S.; Martini, L.; Convertino, D.; Keum, D. H.; Forti, S.; Pezzini, S.; Fabbri, F.; Miseikis, V.; Coletti, C. Synthesis of Large-Scale Monolayer 1T'-$MoTe_2$ and Its Stabilization via Scalable hBN Encapsulation. *ACS Nano* **2021**, *15* (3), 4213−4225.
(45) Han, W.; Liu, K.; Yang, S.; Wang, F.; Su, J.; Jin, B.; Li, H.; Zhai, T. Salt-assisted chemical vapor deposition of two-dimensional materials. *Science China Chemistry* **2019**, *62* (10), 1300−1311.
(46) Aras, F. G.; Yilmaz, A.; Tasdelen, H. G.; Ozden, A.; Ay, F.; Perkgoz, N. K.; Yeltik, A. A review on recent advances of chemical vapor deposition technique for monolayer transition metal dichalcogenides (MX_2: Mo, W; S, Se, Te). *Materials Science in Semiconductor Processing* **2022**, *148*, 106829.
(47) Wu, Q.; Zhang, J.; Tang, L.; Khan, U.; Nong, H.; Zhao, S.; Sun, Y.; Zheng, R.; Zhang, R.; Wang, J.; Tan, J.; Yu, Q.; He, L.; Li, S.; Zou, X.; Cheng, H.-M.; Liu, B. Iodine-assisted ultrafast growth of high-quality monolayer MoS_2 with sulfur-terminated edges. *National Science Open* **2023**, *2* (4), 20230009.
(48) An, B.; Ma, Y.; Chu, F.; Li, X.; Wu, Y.; You, C.; Deng, W.; Li, S.; Zhang, Y. Growth of centimeter scale $Nb_{1-x}W_xSe_2$ monolayer film by promoter assisted liquid phase chemical vapor deposition. *Nano Research* **2022**, *15* (3), 2608−2615.
(49) Zhang, D.; Wen, C.; McClimon, J. B.; Masih Das, P.; Zhang, Q.; Leone, G. A.; Mandyam, S. V.; Drndic, M.; Johnson, A. T. C., Jr.; Zhao, M. Q. Rapid Growth of Monolayer $MoSe_2$ Films for Large-Area Electronics. *Adv. Electron Mater.* **2021**, *7* (6), 2001219.
(50) Wibowo, A. A.; Tebyetekerwa, M.; Bui, A. D.; Kremer, F.; Saji, S.; Yin, Z.; Lu, Y.; Macdonald, D.; Nguyen, H. T. High-Luminescence and Submillimeter-Scale MoS_2 Monolayer Growth Using Combinational Phase Precursors via Chemical Vapor Deposition. *ACS Applied Electronic Materials* **2022**, *4* (10), 5072−5080.
(51) Han, G. H.; Kybert, N. J.; Naylor, C. H.; Lee, B. S.; Ping, J.; Park, J. H.; Kang, J.; Lee, S. Y.; Lee, Y. H.; Agarwal, R.; Johnson, A. T. Seeded growth of highly crystalline molybdenum disulphide monolayers at controlled locations. *Nat. Commun.* **2015**, *6*, 6128.
(52) Hu, Y.; Dai, M.; Feng, W.; Zhang, X.; Zhang, S.; Tan, B.; Shang, H.; Fu, Y. Q.; Hu, P. Monolayer hydrophilic MoS_2 with strong charge trapping for atomically thin neuromorphic vision systems. *Materials Horizons* **2020**, *7* (12), 3316−3324.
(53) Li, G.; Zhang, W.; Zhang, Y.; Lee, Y.; Zhao, Z.; Song, X. Z.; Tan, Z.; Kim, K.; Liu, N. Ammonium Salts: New Synergistic Additive for Chemical Vapor Deposition Growth of MoS_2. *J. Phys. Chem. Lett.* **2021**, *12* (51), 12384−12390.
(54) Yang, J.; Gu, Y.; Lee, E.; Lee, H.; Park, S. H.; Cho, M. H.; Kim, Y. H.; Kim, Y. H.; Kim, H. Wafer-scale synthesis of thickness-controllable MoS_2 films via solution-processing using a dimethylformamide/n-butylamine/2-aminoethanol solvent system. *Nanoscale* **2015**, *7* (20), 9311−9319.
(55) Salazar, R.; Varotto, S.; Vergnaud, C.; Garcia, V.; Fusil, S.; Chaste, J.; Maroutian, T.; Marty, A.; Bonell, F.; Pierucci, D.; Ouerghi, A.; Bertran, F.; Le Fevre, P.; Jamet, M.; Bibes, M.; Rault, J. Visualizing Giant Ferroelectric Gating Effects in Large-Scale $WSe_2/BiFeO_3$ Heterostructures. *Nano Lett.* **2022**, *22* (23), 9260−9267.
(56) Lim, Y. R.; Song, W.; Han, J. K.; Lee, Y. B.; Kim, S. J.; Myung, S.; Lee, S. S.; An, K. S.; Choi, C. J.; Lim, J. Wafer-Scale, Homogeneous MoS2 Layers on Plastic Substrates for Flexible Visible-Light Photodetectors. *Adv. Mater.* **2016**, *28* (25), 5025−5030.
(57) Ionescu, R.; Campbell, B.; Wu, R.; Aytan, E.; Patalano, A.; Ruiz, I.; Howell, S. W.; McDonald, A. E.; Beechem, T. E.; Mkhoyan, K. A.; Ozkan, M.; Ozkan, C. S. Chelant Enhanced Solution Processing for Wafer Scale Synthesis of Transition Metal Dichalcogenide Thin Films. *Sci. Rep* **2017**, *7* (1), 6419.
(58) Wu, Q.; Nong, H.; Zheng, R.; Zhang, R.; Wang, J.; Yang, L.; Liu, B. Resolidified Chalcogen Precursors for High-Quality 2D Semiconductor Growth. *Angew. Chem., Int. Ed.* **2023**, *62*, e202301501.
(59) Zuo, Y.; Yu, W.; Liu, C.; Cheng, X.; Qiao, R.; Liang, J.; Zhou, X.; Wang, J.; Wu, M.; Zhao, Y.; Gao, P.; Wu, S.; Sun, Z.; Liu, K.; Bai, X.; Liu, Z. Optical fibres with embedded two-dimensional materials for ultrahigh nonlinearity. *Nat. Nanotechnol.* **2020**, *15* (12), 987−991.
(60) Qin, B.; Ma, H.; Hossain, M.; Zhong, M.; Xia, Q.; Li, B.; Duan, X. Substrates in the Synthesis of Two-Dimensional Materials via Chemical Vapor Deposition. *Chem. Mater.* **2020**, *32* (24), 10321−10347.
(61) Li, S.; Ouyang, D.; Zhang, N.; Zhang, Y.; Murthy, A.; Li, Y.; Liu, S.; Zhai, T. Substrate Engineering for Chemical Vapor Deposition Growth of Large-Scale Two-Dimensional Transition Metal Dichalcogenides. *Adv. Mater.* **2023**, *35*, e2211855.
(62) Chen, L.; Liu, B.; Ge, M.; Ma, Y.; Abbas, A. N.; Zhou, C. Step-Edge-Guided Nucleation and Growth of Aligned WSe_2 on Sapphire via a Layer-over-Layer Growth Mode. *ACS Nano* **2015**, *9* (8), 8368−8375.
(63) Shi, J.; Huan, Y.; Xiao, M.; Hong, M.; Zhao, X.; Gao, Y.; Cui, F.; Yang, P.; Pennycook, S. J.; Zhao, J.; Zhang, Y. Two-Dimensional Metallic $NiTe_2$ with Ultrahigh Environmental Stability, Conductivity, and Electrocatalytic Activity. *ACS Nano* **2020**, *14* (7), 9011−9020.
(64) Kang, W. T.; Phan, T. L.; Ahn, K. J.; Lee, I.; Kim, Y. R.; Won, U. Y.; Kim, J. E.; Lee, Y. H.; Yu, W. J. Selective Pattern Growth of Atomically Thin $MoSe_2$ Films via a Surface-Mediated Liquid-Phase Promoter. *ACS Appl. Mater. Interfaces* **2021**, *13* (15), 18056−18064.
(65) Qin, Z.; Loh, L.; Wang, J.; Xu, X.; Zhang, Q.; Haas, B.; Alvarez, C.; Okuno, H.; Yong, J. Z.; Schultz, T.; Koch, N.; Dan, J.; Pennycook, S. J.; Zeng, D.; Bosman, M.; Eda, G. Growth of Nb-Doped Monolayer WS_2 by Liquid-Phase Precursor Mixing. *ACS Nano* **2019**, *13* (9), 10768−10775.
(66) Kwon, K. C.; Kim, C.; Le, Q. V.; Gim, S.; Jeon, J. M.; Ham, J. Y.; Lee, J. L.; Jang, H. W.; Kim, S. Y. Synthesis of Atomically Thin Transition Metal Disulfides for Charge Transport Layers in Optoelectronic Devices. *ACS Nano* **2015**, *9* (4), 4146−4155.
(67) Jo, H. K.; Kim, J.; Lim, Y. R.; Shin, S.; Song, D. S.; Bae, G.; Kwon, Y. M.; Jang, M.; Yim, S.; Myung, S.; Lee, S. S.; Kim, C. G.; Kim, K. K.; Lim, J.; Song, W. Wafer-Scale Production of Two-Dimensional Tin Monoselenide: Expandable Synthetic Platform for van der Waals Semiconductor-Based Broadband Photodetectors. *ACS Nano* **2023**, *17* (2), 1372−1380.
(68) Li, S.; Hong, J.; Gao, B.; Lin, Y. C.; Lim, H. E.; Lu, X.; Wu, J.; Liu, S.; Tateyama, Y.; Sakuma, Y.; Tsukagoshi, K.; Suenaga, K.; Taniguchi, T. Tunable Doping of Rhenium and Vanadium into Transition Metal Dichalcogenides for Two-Dimensional Electronics. *Advanced Science* **2021**, *8* (11), 2004438.
(69) Alam, A. U.; Howlader, M. M. R.; Deen, M. J. Oxygen Plasma and Humidity Dependent Surface Analysis of Silicon, Silicon Dioxide and Glass for Direct Wafer Bonding. *ECS Journal of Solid State Science and Technology* **2013**, *2* (12), P515−P523.
(70) Zhang, T.; Fujisawa, K.; Zhang, F.; Liu, M.; Lucking, M. C.; Gontijo, R. N.; Lei, Y.; Liu, H.; Crust, K.; Granzier-Nakajima, T.; Terrones, H.; Elias, A. L.; Terrones, M. Universal In Situ Substitutional Doping of Transition Metal Dichalcogenides by

Liquid-Phase Precursor-Assisted Synthesis. *ACS Nano* **2020**, *14* (4), 4326−4335.
(71) Li, Y.; Hao, S.; DiStefano, J. G.; Murthy, A. A.; Hanson, E. D.; Xu, Y.; Wolverton, C.; Chen, X.; Dravid, V. P. Site-Specific Positioning and Patterning of MoS_2 Monolayers: The Role of Au Seeding. *ACS Nano* **2018**, *12* (9), 8970−8976.
(72) Sun, D.; Nguyen, A. E.; Barroso, D.; Zhang, X.; Preciado, E.; Bobek, S.; Klee, V.; Mann, J.; Bartels, L. Chemical vapor deposition growth of a periodic array of single-layer MoS_2 islands via lithographic patterning of an SiO_2/Si substrate. *2D Materials* **2015**, *2* (4), 045014.
(73) Wang, Z.; Huang, Q.; Chen, P.; Wang, J.; Lu, Y.; Zhang, S.; Liang, X.; Wang, L. Patterned growth of tungsten diselenide flakes by chemical vapor deposition. *Jpn. J. Appl. Phys.* **2017**, *56* (8), 080303.
(74) Pareek, D.; Roach, K. G.; Gonzalez, M. A.; Busing, L.; Parisi, J.; Gutay, L.; Schafer, S. Micro-patterned deposition of MoS_2 ultrathin-films by a controlled droplet dragging approach. *Sci. Rep.* **2021**, *11* (1), 13993.
(75) Li, S.; Lin, Y. C.; Liu, X. Y.; Hu, Z.; Wu, J.; Nakajima, H.; Liu, S.; Okazaki, T.; Chen, W.; Minari, T.; Sakuma, Y.; Tsukagoshi, K.; Suenaga, K.; Taniguchi, T.; Osada, M. Wafer-scale and deterministic patterned growth of monolayer MoS_2 via vapor-liquid-solid method. *Nanoscale* **2019**, *11* (34), 16122−16129.
(76) Lee, J.; Pak, S.; Lee, Y. W.; Park, Y.; Jang, A. R.; Hong, J.; Cho, Y.; Hou, B.; Lee, S.; Jeong, H. Y.; Shin, H. S.; Morris, S. M.; Cha, S.; Sohn, J. I.; Kim, J. M. Direct Epitaxial Synthesis of Selective Two-Dimensional Lateral Heterostructures. *ACS Nano* **2019**, *13* (11), 13047−13055.
(77) Chen, C.; Yang, Y.; Zhou, X.; Xu, W.; Cui, Q.; Lu, J.; Jing, H.; Tian, D.; Xu, C.; Zhai, T.; Xu, H. Synthesis of Large-Area Uniform MoS_2-WS_2 Lateral Heterojunction Nanosheets for Photodetectors. *ACS Applied Nano Materials* **2021**, *4* (5), 5522−5530.
(78) Wu, W.; Zhang, Q.; Zhou, X.; Li, L.; Su, J.; Wang, F.; Zhai, T. Self-powered photovoltaic photodetector established on lateral monolayer MoS_2-WS_2 heterostructures. *Nano Energy* **2018**, *51*, 45−53.
(79) Zhu, J.; Li, W.; Huang, R.; Ma, L.; Sun, H.; Choi, J. H.; Zhang, L.; Cui, Y.; Zou, G. One-Pot Selective Epitaxial Growth of Large WS_2/MoS_2 Lateral and Vertical Heterostructures. *J. Am. Chem. Soc.* **2020**, *142* (38), 16276−16284.
(80) Vu, V. T.; Vu, T. T. H.; Phan, T. L.; Kang, W. T.; Kim, Y. R.; Tran, M. D.; Nguyen, H. T. T.; Lee, Y. H.; Yu, W. J. One-Step Synthesis of $NbSe_2$/Nb-Doped-WSe_2 Metal/Doped-Semiconductor van der Waals Heterostructures for Doping Controlled Ohmic Contact. *ACS Nano* **2021**, *15* (8), 13031−13040.
(81) Kozhakhmetov, A.; Schuler, B.; Tan, A. M. Z.; Cochrane, K. A.; Nasr, J. R.; El-Sherif, H.; Bansal, A.; Vera, A.; Bojan, V.; Redwing, J. M.; Bassim, N.; Das, S.; Hennig, R. G.; Weber-Bargioni, A.; Robinson, J. A. Scalable Substitutional Re-Doping and its Impact on the Optical and Electronic Properties of Tungsten Diselenide. *Adv. Mater.* **2020**, *32* (50), e2005159.
(82) Fan, S.; Yun, S. J.; Yu, W. J.; Lee, Y. H. Tailoring Quantum Tunneling in a Vanadium-Doped WSe_2/$SnSe_2$ Heterostructure. *Advanced Science* **2020**, *7* (3), 1902751.
(83) Loh, L.; Chen, Y.; Wang, J.; Yin, X.; Tang, C. S.; Zhang, Q.; Watanabe, K.; Taniguchi, T.; Wee, A. T.; Bosman, M.; Quek, S. Y.; Eda, G. Impurity-Induced Emission in Re-Doped WS_2 Monolayers. *Nano Lett.* **2021**, *21* (12), 5293−5300.
(84) Wang, C.; Xu, L.; Jin, H.; Li, C.; Zhang, Z.; Li, L.; Chen, Y.; Su, J.; Liu, N.; Lai, J.; Long, F.; Jiang, X.; Gao, Y. Yb/Er coordinatively doping in bilayer WSe_2 for fascinating up-conversion luminescence. *Nano Energy* **2020**, *78*, 105317.
(85) Taniguchi, T.; Nurdiwijayanto, L.; Li, S.; Lim, H. E.; Miyata, Y.; Lu, X.; Ma, R.; Tang, D. M.; Ueda, S.; Tsukagoshi, K.; Sasaki, T.; Osada, M. On/Off Boundary of Photocatalytic Activity between Single- and Bilayer MoS_2. *ACS Nano* **2020**, *14* (6), 6663−6672.
(86) Son, E.; Lee, S.; Seo, J.; Kim, U.; Kim, S. H.; Baik, J. M.; Han, Y. K.; Park, H. Engineering the Local Atomic Configuration in 2H TMDs for Efficient Electrocatalytic Hydrogen Evolution. *ACS Nano* **2023**, *17* (11), 10817−10826.
(87) Zhang, F.; Zheng, B.; Sebastian, A.; Olson, D. H.; Liu, M.; Fujisawa, K.; Pham, Y. T. H.; Jimenez, V. O.; Kalappattil, V.; Miao, L.; Zhang, T.; Pendurthi, R.; Lei, Y.; Elias, A. L.; Wang, Y.; Alem, N.; Hopkins, P. E.; Das, S.; Crespi, V. H.; Phan, M. H.; Terrones, M. Monolayer Vanadium-Doped Tungsten Disulfide: A Room-Temperature Dilute Magnetic Semiconductor. *Advanced Science* **2020**, *7* (24), 2001174.
(88) Pham, Y. T. H.; Liu, M.; Jimenez, V. O.; Yu, Z.; Kalappattil, V.; Zhang, F.; Wang, K.; Williams, T.; Terrones, M.; Phan, M. H. Tunable Ferromagnetism and Thermally Induced Spin Flip in Vanadium-Doped Tungsten Diselenide Monolayers at Room Temperature. *Adv. Mater.* **2020**, *32* (45), e2003607.
(89) Yun, S. J.; Duong, D. L.; Ha, D. M.; Singh, K.; Phan, T. L.; Choi, W.; Kim, Y. M.; Lee, Y. H. Ferromagnetic Order at Room Temperature in Monolayer WSe_2 Semiconductor via Vanadium Dopant. *Adv. Sci. (Weinh)* **2020**, *7* (9), 1903076.
(90) Lai, Y.; Tan, J.; Cai, Z.; Zhang, R.; Teng, C.; Zhao, S.; Lin, J.; Liu, B. Dissolution−precipitation growth of doped monolayer molybdenum disulfide through double-faced precursor supply. *APL Materials* **2021**, *9* (5), 051123.
(91) Kang, W. T.; Lee, I. M.; Yun, S. J.; Song, Y. I.; Kim, K.; Kim, D. H.; Shin, Y. S.; Lee, K.; Heo, J.; Kim, Y. M.; Lee, Y. H.; Yu, W. J. Direct growth of doping controlled monolayer WSe_2 by selenium-phosphorus substitution. *Nanoscale* **2018**, *10* (24), 11397−11402.
(92) Liu, X.; Jiang, X.; Shao, G.; Xiang, H.; Li, Z.; Jin, Y.; Chen, Y.; Jiang, H.; Li, H.; Shui, J.; Feng, Y.; Liu, S. Activating the Electrocatalysis of MoS_2 Basal Plane for Hydrogen Evolution via Atomic Defect Configurations. *Small* **2022**, *18* (22), e2200601.
(93) Shen, D.; Zhao, B.; Zhang, Z.; Zhang, H.; Yang, X.; Huang, Z.; Li, B.; Song, R.; Jin, Y.; Wu, R.; Li, B.; Li, J.; Duan, X. Synthesis of Group VIII Magnetic Transition-Metal-Doped Monolayer $MoSe_2$. *ACS Nano* **2022**, *16* (7), 10623−10631.
(94) Zhou, J.; Lin, J.; Sims, H.; Jiang, C.; Cong, C.; Brehm, J. A.; Zhang, Z.; Niu, L.; Chen, Y.; Zhou, Y.; Wang, Y.; Liu, F.; Zhu, C.; Yu, T.; Suenaga, K.; Mishra, R.; Pantelides, S. T.; Zhu, Z. G.; Gao, W.; Liu, Z.; Zhou, W. Synthesis of Co-Doped MoS_2 Monolayers with Enhanced Valley Splitting. *Adv. Mater.* **2020**, *32* (29), e1906536.
(95) Yun, W. S.; Lee, J. D. Unexpected strong magnetism of Cu doped single-layer MoS_2 and its origin. *Phys. Chem. Chem. Phys.* **2014**, *16* (19), 8990−8996.
(96) Fan, X.-L.; An, Y.-R.; Guo, W.-J. Ferromagnetism in Transitional Metal-Doped MoS_2 Monolayer. *Nanoscale Res. Lett.* **2016**, *11* (1), 1−10.
(97) Li, B.; Xing, T.; Zhong, M.; Huang, L.; Lei, N.; Zhang, J.; Li, J.; Wei, Z. A two-dimensional Fe-doped SnS_2 magnetic semiconductor. *Nat. Commun.* **2017**, *8* (1), 1958.
(98) Yang, L.; Wu, H.; Zhang, L.; Zhang, W.; Li, L.; Kawakami, T.; Sugawara, K.; Sato, T.; Zhang, G.; Gao, P.; Muhammad, Y.; Wen, X.; Tao, B.; Guo, F.; Chang, H. Highly Tunable Near-Room Temperature Ferromagnetism in Cr-Doped Layered Td-WTe_2. *Adv. Funct. Mater.* **2021**, *31* (13), 2008116.
(99) Yang, L.; Wu, H.; Zhang, L.; Zhang, G.; Li, H.; Jin, W.; Zhang, W.; Chang, H. Tunable and Robust Near-Room-Temperature Intrinsic Ferromagnetism of a van der Waals Layered Cr-Doped 2H-$MoTe_2$ Semiconductor with an Out-of-Plane Anisotropy. *ACS Appl. Mater. Interfaces* **2021**, *13* (27), 31880−31890.
(100) Yun, S. J.; Cho, B. W.; Dinesh, T.; Yang, D. H.; Kim, Y. I.; Jin, J. W.; Yang, S. H.; Nguyen, T. D.; Kim, Y. M.; Kim, K. K.; Duong, D. L.; Kim, S. G.; Lee, Y. H. Escalating Ferromagnetic Order via Se-Vacancies Near Vanadium in WSe_2 Monolayers. *Adv. Mater.* **2022**, *34* (10), e2106551.

https://doi.org/10.1021/prechem.3c00115
Precis. Chem. 2024, 2, 282−299